A two-scale model for an array of AFM's cantilever in the static case

M. Lenczner* and R.C Smith†

June 19, 2006

Abstract

The primary objective of this paper is to present a simplified model for an array of Atomic Force Microscopes (AFM) operating in static mode. Its derivation is based on the asymptotic theory of thin plates initiated by P. Ciarlet and P. Destuynder and on the two-scale convergence introduced by M. Lenczner which generalizes the theory of G. Nguetseng and G. Allaire. As an example, we investigate in full detail a particular configuration, which leads to a very simple model for the array. Aspects of the theory for this con&guration are illustrated through simulation results. Finally the formulation of our theory of two-scale convergence is fully revisited. All the proofs are reformulated on a significantly simpler manner.

1 Introduction

In recent years, a number of new Microsystems or Nanosystems Array architectures have been developed. These architectures include microcantilevers, micromirrors, droplets ejectors, micromembranes, microresistors, biochips, nanodots, nanowires to cite only few and application are continually emerging in numerous areas of science and technology. In some of these systems, units have a collective behavior whereas in others they are working individually. However, in all cases their coupling is an important design parameter of the array that is promoted or avoided. The coupling can be of various natures including mechanical, thermal and electromagnetic. The numerical simulation of such whole arrays based on classical methods like Finite Element Methods (FEM) is prohibitive for today's computers at least in a time compatible with the time scale of a designer. Indeed, the calculation of a reasonably complex cell of a three dimensional Microsystems requires about 10^3 degrees of freedoms which leads to about 10^7 degrees of freedoms for a 100×100 array. Moreover usual Microsystems involves strong nonlinearities that cannot be ignored.

This work is focused on a relatively simple example of Microsystems Array, namely an Atomic Force Microscopes Array (AFMA). A number of developments of AFMA or of more simple Cantilever Arrays have already been achieved, as noted in the abbreviated set of citations [29]-[62].

*Center for Research in Scientific Computation, North Carolina State University, Raleigh, NC 27695. E-mail address: michel.lenczner@utbm.fr.

†Center for Research in Scientific Computation, North Carolina State University, Raleigh, NC 27695. E-mail address: rsmith@eos.ncsu.edu

The modeling of single AFM has been extensively studied in the literature in many different configurations, as noted in the review papers [14], [21] and [13]. Most of the models are based on a spring-damper-mass model where the precise features of the mechanical systems are ignored. More careful modeling has been derived in various situations including tapping mode, interaction with a surrounding fluid; see [16]-[23]. They are based on the Euler-Bernoulli beam model with an applied force at the extremity of the beam except in [12] where the tip is modeled as a rigid part and the force is applied to it. Until now, with the best of our knowledge, only the group of B. Bamieh, see [24] and the reference therein, has published a model of coupled cantilever array. These authors take into account the electrostatic coupling with a rudimentary derivation.

To simplify the discussion we focus on the simplest case of an AFMA in static operation. We establish a two-dimensional thin plate model for an elastic component including a rigid part corresponding to the tip that is assumed to be much stiffer than the supple part of the cantilever. Then a simplified model of an array of AFMs coupled through their base is derived from the thin plate model. Each of these models is illustrated by an example. Analytic calculations are conducted to yield very simple formulations. Finally a numerical simulation of the array is presented and discussed. The derivations of the two models are rigorously justified through asymptotic methods. The thin plate model is based on the asymptotic methods of P. Ciarlet [2] and P. Destuynder [1] as well as on our previous work [6]. The derivation of the AFMA two-scale model uses the two-scale transform and convergence introduced by one of the author, see [15], [11] and [10]. However it is completely reformulated in a simpler and more intuitive manner.

We note that for the geometry considered in this paper, our two-scale convergence is equivalent to the two-scale convergence of G. Nguetseng [7] and G. Allaire [5]. However it is worthwhile to remark that it has the of working also for electrical circuit homogenization (as a particular case of $d-n$ dimensional periodic manifolds immersed in a $d-$dimensional space) when the other doesn$'$t apply as it has also been recognized in [9]. This remark constitutes an encouragement to develop this method in the framework of Mechatronical Systems. We point out that these methods are in the vein of the homogenization methods by E. Sanchez-Palencia [3], L. Tartar and A. Bensoussan, J.L. Lions, G. Papanicolaou [4]. Finally, we cite the work of G. Griso and his coworkers initiated in [8] who have rediscovered the same method and named it the Unfolding Method.

We review the main features of the simplified models presented in this paper. Simply stated, an AFM evaluates the interaction force between the tip and the sample through the deformation measurement of the supple part of the cantilever. To do so, the tip is designed so that its deformation is very weak so that it efficiently transmit the energy of deformation. This is why we assume that the tip is perfectly rigid. This asumption simplifies significantly the model by reducing the number of degree of freedom. Then, the thin plate model is derived under the assumption that in the one side the supple part of the cantilever is very thin and in the same time that the tip is also thin, both with the same order of magnitude. The AFMA is constituted of cantilevers clamped in a common base. For the model derivation, we assume that the base is much stiffer that the cantilever. This is expressed by saying that their stiffness have different asymptotic behavior. Doing this, the effective stiffness of the base in the homogenized model is not affected by the presence of the cantilever and so is independent of the tip-sample forces (that produce nonlinearities). This is an appreciable simplification. In the example that we detail, the base and the cantilevers are rectangular. The tip-sample forces are the van der Waals forces and the chemical interaction forces. In this case the model is in the

one side a fourth order one-dimensional boundary value problem related to the deflection in the base coupled with the model of the cantilever at the micro-scale which reduces to a single nonlinear algebraic equation related to the tip-sample distance. The numerical simulations are conducted for simple sample profiles: flat, slope and a quadratic shape. The tip-sample distance is a distributed variable along the array that we discretize with Chebychev polynomials. The numerical experiments show that even for simple sample shapes, a relatively large number of polynomials are required for an accurate approximation. It is also observed that even for a moderate number of cantilevers the deflection of the base is far from being negligible in comparison with the tip displacement. This is due to the fact that the deflection increases when the length of the base increase as its fourth power.

We note that the derivation of a two-scale model for the evolution problem can be directly deduced from the static model. However the dynamic problem requires much dedicated analysis, simulations and discussions so that we have chosen to postpone its presentation until a further publication.

The paper is organized as follows. We establish aspects of the geometry and nature of tip forces in the remainder of this section. The three-dimensional elastic model coupled with a rigid part is stated and derived in Section 2. The thin plate model is stated and derived in Section 3. The two-scale model is stated and derived in Section 4. It is based on the two-scale theory presented in the appendix postponed in Section 7. The examples and the numerical simulations are reported in Section 6.

2 Three-Dimensional Model

We start by considering a mechanical structure located in $\Omega \subset \mathbb{R}^3$ made up of an elastic part and a rigid part located respectively in Ω_E and in Ω_R as depicted in Figure 1. The model is stated in the next section and subsequently justified in Section 2.2.

2.1 Statement of the Model

The elastic component is clamped along part of its boundary Γ_0, is linked to the rigid part through the interface $\Gamma_{E,R}$ and is free of applied forces in the remaining part Γ_1. When the system is totally elastic (no rigid part), then Ω_R and $\Gamma_{E,R}$ are void and the related equation must be ignored. The mechanical displacements are denoted by the vector $u = (u_1, u_2, u_3)^T$ defined over the entire structure.

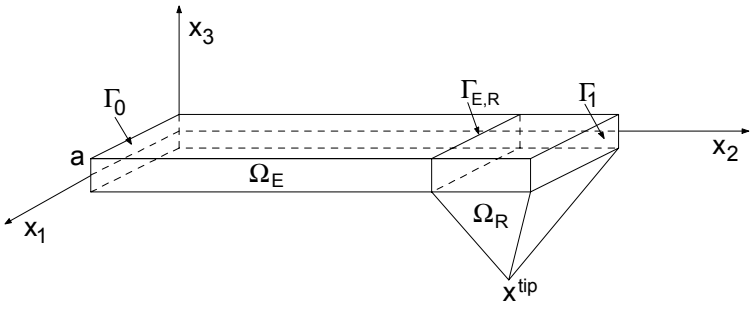

Figure 1: Three-dimensional plate with the rigid part

The fourth-order elasticity tensor is denoted by R and may vary in space if the material is not homogeneous. The symmetric matrix of linear strains is $s(u) = \frac{1}{2}(\nabla u + \nabla^T u)$ where ∇

is the gradient operator. The equilibrium equations, the linear stress-strains relation and the rigidity constraint are stated as

$$-div(\sigma) = f,\ \sigma = Rs(u) \text{ in } \Omega_E \text{ and } s(u) = 0 \text{ in } \Omega_R \tag{1}$$

where the product between the fourth-order tensor R and the matrix $s(u)$ gives the 3×3 matrix with entries

$$\sigma_{ij} = \sum_{k,l=1}^{3} R_{ijkl} s_{kl}(u).$$

In the case of isotropic elasticity, the elasticity tensor has the form

$$R_{ijkl} = \lambda\delta_{ij}\delta_{kl} + 2\mu\delta_{ik}\delta_{jl}$$

where δ is the Kronecker delta.

The boundary conditions are $u = 0$ on Γ_0, $\sigma n = 0$ on Γ_1 (n being the outward normal vector to the boundary). Moreover, u will be continuous at the interface $\Gamma_{E,R}$. Finally, the force and force momentum transmissions satisfy

$$\int_{\Gamma_{E,R}} \sigma\ n\ ds = \xi,\ \int_{\Gamma_{E,R}} (\sigma\ n).(x \times e_k)\ ds = \Xi_k \text{ for } k \in \{1,2,3\} \tag{2}$$

where

$$\xi = \int_{\Omega_R} f(x)dx,\ \Xi_k = \int_{\Omega_R} f(x).(x \times e_k)dx.$$

We note that the condition $s(u) = 0$ can be formulated through imposing a rigid displacement $u = b + x \times B$ whose b and B are some three dimensional vectors. The variational formulation, which is necessary for the formulation of Galerkin-like numerical methods, can be formulated as follows: find $u \in V$ such that

$$\int_{\Omega_E} \sigma :: s(v)\ dx = \int_{\Omega} f.v\ dx \tag{3}$$

for all $v \in V$ for the previous stress-strains relationship where the admissible space of test functions is

$$V = \{v \in H^1(\Omega)^3\ /\ s(v) = 0 \text{ in } \Omega_R \text{ and } v = 0 \text{ on } \Gamma_0\}.$$

The Sobolev space $H^1(\Omega)$ is the set of square integrable functions in Ω, $\int_\Omega v^2(x)\ dx < \infty$, such that each component of their gradient are also square integrable.

2.2 Justification of the Three-Dimensional Model

Consider a sequence of elastic structures filling up Ω so that its rigidity in Ω_R tends to infinity. Namely, the sequence of elasticity tensors has the form $R^n = R$ in Ω_E and $R^n = nR$ in Ω_R where n varies in $\mathbb{N}^*$ from one to infinity. The variational formulation of such a sequence of elastic problem is as follows: find $u^n \in V_E$

$$\int_{\Omega} [R^n s(u^n)] :: s(v)\ dx = \int_{\Omega} f.v\ dx$$

for all $v \in V_E$ where

$$V_E = \{v \in H^1(\Omega)^3 \ / \ v = 0 \text{ on } \Gamma_0\}.$$

Using classical estimates, one may prove that $||\nabla u^n||^2_\Omega$ and $n||s(u^n)||^2_{\Omega_R}$ are bounded uniformly with respect to n where $||v||^2_\Omega = \int_\Omega v^2(x)\ dx$.

The uses of theses estimates justifies the expansion $u^n = u + O(1/n)$ with u independent of n and satisfying $s(u) = 0$ in Ω_R and $s = s(u)$ in Ω_E. Taking n to infinity in the variational formulation and posing $v = 0$ in Ω_R, it follows that u solves the variational formulation (3). The derivation of the local form of the variational formulation (3) is a routine and is not detailed here.

3 A Thin Plate Model

The cantilever of an AFM is comprised of a thin plate equipped with a tip as depicted in Figure 1. The thin plate is assumed to be elastic and the tip is modelled by a rigid body. A simplified model, based on the classical Love-Kirchhoff elastic thin plate theory, is stated in the forthcoming section and its justification is made in Section 3.2.

3.1 Statement of the Model

Because the elastic component is a thin elastic plate with thickness $2a$ and mean section ω_E; we consider the domain

$$\Omega_E = \{x \in \mathbb{R}^3 \ / \ (x_1, x_2) \in \omega_E, \ -a < x_3 < a\}. \tag{4}$$

The three parts Γ_0, Γ_1 and $\Gamma_{E,R}$ of its boundary are parameterized in a similar manner by referring to the corresponding boundaries γ_0^P, γ_1^P and $\gamma_{E,R}^P$ of ω_E. The rigid part is parameterized as

$$\Omega_R = \{x \in \mathbb{R}^3 \ / \ (x_1, x_2) \in \omega_R \text{ with } -h(x_1, x_2) < x_3 < a\}. \tag{5}$$

When a is small enough the three-dimensional model can be simplified to a thin plate model. To justify it, we make some assumptions on the order of magnitude of the applied forces with respect to the thickness a:

$$f_{\alpha=1,2} = O(1),\ a^{-1}f_3 = O(1) \text{ in } \Omega \text{ and } a^{-1}h = O(1) \text{ in } \Omega_R. \tag{6}$$

It then follows that

$$u_\alpha = u_\alpha^P + O(a) \text{ and } au_3 = au_3^P + O(a) \text{ in } \Omega \tag{7}$$

where $O(a)$ is any vanishing quantity when a vanishes and u^P satisfies the Love-Kirchhoff kinematic relations

$$\partial_3 u_3^P = 0,\ u_\alpha^P = \overline{u}_\alpha^P - x_3\partial_{x_\alpha} u_3^P \text{ with } \partial_3 \overline{u}_\alpha^P = 0 \text{ for } \alpha = 1, 2 \text{ in } \Omega_E.$$

In this paper, we neglect the contribution of the membrane displacement $\overline{u}^P$ so we state only the model satisfied by the transverse displacement u_3^P. It is governed by the equilibrium equations, the stress-strains relations and the rigidity constraint

$$div(div(M^P)) = f^P + div(g^P),\ M^P = R^P\nabla\nabla^T u_3^P \text{ in } \omega_E \text{ and } u_3^P = b^P + B^P.x \text{ in } \omega_R \tag{8}$$

where

$$g^P_\alpha(x_1,x_2)=\int_{-a}^{a} f_\alpha(x)x_3\ dx_3 \text{ and } f^P(x_1,x_2)=\int_{-a}^{a} f_3(x)\ dx_3 \text{ in } \omega_E. \tag{9}$$

In the case of isotropic materials, the elasticity can be formulated as

$$R^P_{\alpha\beta\gamma\rho}=a^3\left(\frac{4\lambda\mu}{3(\lambda+2\mu)}\delta_{\alpha\beta}\delta_{\gamma\rho}+\frac{4\mu}{3}\delta_{\alpha\gamma}\delta_{\beta\rho}\right). \tag{10}$$

In addition, $x=(x_1,x_2)^T$, b^P is a scalar and B^P is a two-dimensional vector.

The boundary conditions are

$$\begin{gathered} u^P_3=\nabla u^P_3.n=0 \text{ on } \gamma^P_0 \\ \text{and } n^TM^Pn=0,\ \nabla(n^TM^P\tau).\tau+div(M^P).n=g^P.n \text{ on } \gamma^P_1 \end{gathered} \tag{11}$$

where n and τ are the unit outward normal and the unit tangent to the boundary of ω_E. The transmission condition at the interface $\gamma_{E,R}$ results from the continuity conditions of the displacement u^P_3 and of its gradient ∇u^P_3 and the continuity of the normal stresses. These can be expressed as

$$\begin{gathered} b^P=|\gamma_{E,R}|^{-1}\int_{\gamma_{E,R}}(u^P_3-\nabla u^P_3.x)_{|\omega_E}\ ds,\ B^P=|\gamma_{E,R}|^{-1}\int_{\gamma_{E,R}}(\nabla u^P_3)_{|\omega_E}\ ds \\ -\int_{\gamma_{E,R}} div(M^P).n\ ds=\xi^P \text{ and } \int_{\gamma_{E,R}} n^TM^P-(div(M^P).n)x\ ds=\Xi^P \end{gathered} \tag{12}$$

where

$$\xi^P=-\int_{\gamma_{E,R}}(g^P.n)_{|\omega_E}\ ds+\int_{\omega_R} f^P\ dx,\ \Xi^P_\alpha=-\int_{\gamma_{E,R}}(g^P.n)_{|\omega_E}x_\alpha\ ds+\int_{\omega_R} f^Px_\alpha-g^P_\alpha\ dx,$$

$|\gamma_{E,R}|$ denotes the length of the interface $\gamma_{E,R}$, g^P and f^P having been defined in ω_E and are defined in ω_R by

$$g^P_\alpha(x_1,x_2)=\int_{-h(x_1,x_2)}^{a} f_\alpha(x)x_3\ dx_3 \text{ and } f^P(x_1,x_2)=\int_{-h(x_1,x_2)}^{a} f_3(x)\ dx_3 \text{ in } \omega_R.$$

The variational formulation associated with this model is

$$u^P_3\in V^P \text{ and } \int_{\omega_E} M^P::\nabla\nabla^Tv\ dx=\int_{\omega_P} f^Pv-g^P.\nabla v\ dx \text{ for all } v\in V^P \tag{13}$$

taking into account the stress-strains relation. The set of admissible transverse displacements is

$$V^P=\{v\in H^2(\omega_P)\ /\ \nabla\nabla^Tv=0 \text{ in } \omega_R \text{ and } v=0 \text{ on } \gamma^P_0\}$$

and $H^2(\omega_P)$ being the set of square integrable functions on ω_P so that their first order and second order derivatives are also square integrable.

Remark 1 *For the derivation of the two-scale model, we need an extension of this model for plates with varying thickness, namely, when Ω_E and Ω_R are replaced by*

$$\begin{aligned} \Omega_E &= \{x\in\mathbb{R}^3\ /\ (x_1,x_2)\in\omega_E \text{ and } -k(x_1,x_2)<x_3<k(x_1,x_2)\} \\ \Omega_R &= \{x\in\mathbb{R}^3\ /\ (x_1,x_2)\in\omega_R \text{ with} -h(x_1,x_2)<x_3<k(x_1,x_2)\} \end{aligned}$$

where k is a positive function so that $a^{-1}k=O(1)$. In such a case, the model remains the same excepted that a is replaced by k in the expressions of the two-dimensional forces (9) and of the two-dimensional rigidities (10).

3.2 Justification of the Thin Plate Model

The justification of the thin plate model is based on the asymptotic method of P.G. Ciarlet [2] and of P. Destuynder [1]. In these works, the thin plate model is derived for isotropic elastic bodies by calculating the asymptotic behavior of the elasticity system and of its solution when the parameter a vanishes. In this work we use the same method but our derivation is based on the paper E. Canon and M. Lenczner [6] where material anisotropy was encompassed. The only difference between the new model and that in [6] comes from the presence of the rigid body which does not significantly affect the proofs. Hence we report only the main steps in the calculations.

Since the asymptotic method consist of finding the limit when a vanishes, it is mandatory to introduce a scaled domain independent of a and to formulate the problem on it. To do so, one introduces the change of variable F^a defined on Ω by $F^a(x) = (x_1, x_2, \frac{1}{a}x_3)$ in Ω. The image $F^a(\Omega)$ is denoted by $\widetilde{\Omega}$ and there the coordinates are $\widetilde{x} = F^a(x)$. The whole model is now expressed on the dilated domain. All variables or fields related to $\widetilde{\Omega}$ are covered by a tilde. The rigidity, the mechanical displacement and the forces are scaled in different manners

$$\widetilde{R}(\widetilde{x}) = R(x),\ \widetilde{u}(\widetilde{x}) = (u_1, u_2, au_3)(x),\ \widetilde{f}(\widetilde{x}) = (f_1, f_2, \frac{1}{a}f_3)(x) \text{ for } x \in \Omega.$$

From the assumption made on f, it is clear that $||\widetilde{f}||_{\widetilde{\Omega}}$ is bounded. We also apply a scaling to the test functions

$$\widetilde{v}(\widetilde{x}) = (v_1, v_2, av_3)(x).$$

For a given displacement field v, define the 3×3 matrice $K(\widetilde{v})$ such that $K_{\alpha\beta}(\widetilde{v}) = s_{\alpha\beta}(\widetilde{v})$, $K_{\alpha 3}(\widetilde{v}) = K_{3\alpha}(\widetilde{v}) = a^{-1}s_{3\alpha}(\widetilde{v})$ and $K_{33}(\widetilde{v}) = a^{-2}s_{33}(\widetilde{v})$. Applying the variable change $\widetilde{x} = F^a(x)$ in (3) yields the following variational formulation: find $\widetilde{u} \in \widetilde{V}$ such that

$$a\int_{\widetilde{\Omega}_E} \widetilde{\sigma} :: K(\widetilde{v})\ d\widetilde{x} = a\int_{\widetilde{\Omega}} \widetilde{f}(\widetilde{x}).\widetilde{v}(\widetilde{x})\ d\widetilde{x} \tag{14}$$

for all $\widetilde{v} \in \widetilde{V}$ where $\widetilde{\sigma} = \widetilde{R}K(\widetilde{u})$ and

$$\widetilde{V} = \{\widetilde{v} \in H^1(\widetilde{\Omega})^3 \ /\ K(\widetilde{v}) = 0 \text{ in } \widetilde{\Omega}_R \text{ and } \widetilde{v} = 0 \text{ on } \widetilde{\Gamma}_0\}.$$

By equating $\widetilde{v} = \widetilde{u}$, one may prove that $||\widetilde{u}||_{\widetilde{\Omega}}$ and $||K(\widetilde{u})||_{\widetilde{\Omega}}$ are $O(1)$ with respect to a. Thus we are led to formulate

$$\widetilde{u} = \widetilde{u}^P + O(a),\ K(\widetilde{u}) = K^P + O(a)$$

where $\widetilde{u}^P$ and K^P are independent of a. It follows that

$$K^P_{\alpha\beta} = s_{\alpha\beta}(\widetilde{u}^P) \text{ for } \alpha, \beta = 1, 2 \text{ and that } s_{i3}(\widetilde{u}^P) = 0 \text{ for } i = 1, 2, 3.$$

This is equivalent to saying that $\widetilde{u}^P$ fulfils the Love-Kirchhoff kinematics

$$\partial_{\widetilde{x}_3}\widetilde{u}^P_3 = 0 \text{ and } \widetilde{u}^P_\alpha = \widetilde{\overline{u}}^P_\alpha - \widetilde{x}_3\partial_{x_\alpha}\widetilde{u}^P_3 \text{ with } \partial_{\widetilde{x}_3}\widetilde{\overline{u}}^P_\alpha = 0.$$

When neglecting the membrane displacement $\widetilde{\overline{u}}_\alpha$, it appears that $\widetilde{u}^P_3$ solves the variational formulation, which is independent of the parameter a,

$$\widetilde{u}_3^P \in V^P,\ \int_{\omega_E} \widetilde{M}^P :: \nabla\nabla^T \widetilde{v}_3\ d\widetilde{x} = \int_{\widetilde{\Omega}} \widetilde{f}_3\ \widetilde{v}_3 - \widetilde{x}_3 \widetilde{f}_\alpha \partial_{\widetilde{x}_\alpha} \widetilde{v}_3\ d\widetilde{x} \text{ for all } \widetilde{v}_3 \in V^P.$$

Here $\widetilde{M}^P = \widetilde{R}^P \nabla\nabla^T \widetilde{u}_3^P$ and $\widetilde{R}^P$ is defined under the name Q^{22} in E. Canon and M. Lenczner [6] and is equal to

$$\widetilde{R}^P_{\alpha\beta\gamma\rho} = \frac{4\lambda\mu}{3(\lambda+2\mu)}\delta_{\alpha\beta}\delta_{\gamma\delta} + \frac{4\mu}{3}\delta_{\alpha\gamma}\delta_{\beta\rho}$$

in the case of an isotropic material. Applying the inverse variable change, u_3^P solves the variational formulation: find $u_3^P \in V^P$ such that

$$\int_{\omega_E} M^P :: \nabla\nabla^T v_3\ dx = \int_\Omega (f_3\ v_3 - x_3 f_\alpha \partial_{x_\alpha} v_3)\ dx$$

for all $v_3 \in V^P$ with $M^P = R^P \nabla\nabla^T u_3^P$ and $R^P = a^3 \widetilde{R}^P$. This leads directly to the variational formulation (13). Since $\nabla\nabla^T v_3 = 0$ in Ω_R it may be written $v_3 = d + D.x$ with $D = (D_1, D_2)^T$ thus the right hand side may be reformulated as

$$\int_{\omega_E} (f^P\ v_3 - g^P.\nabla v_3)\ dx + \xi^P d^P + \Xi^P.D^P.$$

Application of twice Green formula and using the fact that $v_3 = d + D.x$ on $\gamma_{E,R}$, it follows that

$$\begin{aligned}
&\int_{\omega_E} div(div(M^P) v_3\ dx + \int_{\gamma_1} (n^T M^P \nabla v_3 - div(M^P).n\ v_3)\ ds \\
-(&\int_{\gamma_{E,R}} div(M^P).n\ ds)\ d^P + (\int_{\gamma_{E,R}} (n^T M^P - div(M^P).n\ x)\ ds).D^P \\
&= \int_{\omega_E} (f_3^P + div(g^P)) v_3\ dx - \int_{\gamma_1} g^P.n\ v_3\ ds + \xi^P d^P + \Xi^P.D^P
\end{aligned}$$

from which we deduce all the model equations excepted the continuity condition of u_3^P and ∇u_3^P that comes by integrating the expressions $u_3^P = b^P + B^P.x$ and $\nabla u_3^P = B^P$ on $\gamma_{E,R}$.

4 Model for an AFM Array

Consider a mechanical structure made of a periodic distribution of microcantilevers as shown on Figure 2. In Section 4.1 a simplified model is stated when its derivation is done in Section 4.2.

4.1 Statement of the Model

The whole domain occupied by the cantilever array is still denoted by ω_P and is assumed to be embedded in the macroscopic domain $\omega = (0, L_1) \times (0, L_2)$. It is constituted of $n \times n$ square cells Y_i^ε of size $\varepsilon \times \varepsilon$ and fills up ω which constrains the parameter ε to be equal to $1/n$.

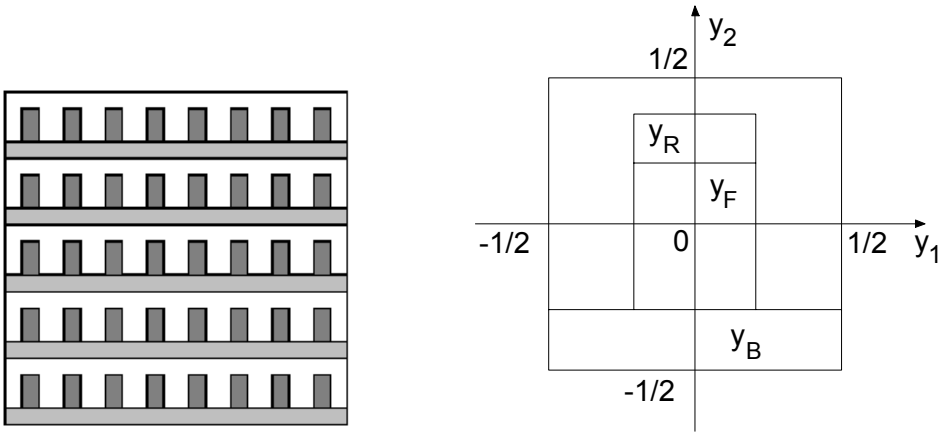

Figure 2: Array of cantilevers and their reference cell

The dilatation and shift of any cell Y_i^ε gives rise to a reference unit cell $Y \subset (-\frac{1}{2}, \frac{1}{2})^2$. For the derivation of the array model, we assume that $\varepsilon/L_1 << 1$. As ω_P, this microscopic cell is comprised of a thin elastic plate Y_E and a rigid part Y_R. In Y_E, we distinguish the base Y_B and the elastic part of the cantilever Y_F that is assumed to be much more flexible than the base. The entire cantilever, made up of Y_F and of the rigid part Y_R, is denoted by Y_C. In ω, the bases and the cantilevers are respectively denoted by ω_B and ω_C.

Consider a function v defined on ω. Its two-scale transform $\widehat{v}(x,y)$ is the function defined on $\omega \times Y$ by

$$\widehat{v}(x,y) = \sum_i \chi_{Y_i^\varepsilon}(x) v(x_i^\varepsilon + \varepsilon y) \tag{15}$$

where the sum holds for all the cells $Y_i^\varepsilon \subset \omega$, x_i^ε are the centers of those cells and $\chi_{Y_i^\varepsilon}$ is the characteristic function of Y_i^ε. The two-scale transform of a function v defined in ω_P only is accomplished through the same definition but after having extended v by zero to ω. The assumptions as well as the model are stated on the two-scale transforms of the various fields playing a role. We quantify the fact that Y_F is much more supple than the base by saying that both

$$\varepsilon^{-4}\widehat{R}^P = R^C + O(\varepsilon) \text{ in } Y_F \text{ and } \widehat{R}^P = R^B + O(\varepsilon) \text{ in } Y_B$$

with R^C and R^B independent of ε. In other word, we consider that the plate has a varying thickness which is equal to $2a_B$ in Y_B and $2a_C$ in Y_C with the ratio $a_C^3/a_B^3 \sim \varepsilon^4$. The thin plate model with varying thickness has been discussed in the Remark 1. In addition, we are led to assume that

$$\widehat{f}^P = f^0 + O(\varepsilon) \text{ in } Y,\ \widehat{g}^P = g^B + O(\varepsilon) \text{ in } Y_B \text{ and } \varepsilon^{-1}\widehat{g}^P = g^C + O(\varepsilon) \text{ in } Y_C$$

with f^0, g^B and g^C independent of ε. Based on these assumptions in ω_B, it follows that

$$\begin{aligned} u_3^P &= u^M + O(\varepsilon),\ \nabla u_3^P = D(u^M,\theta) + O(\varepsilon) \\ \text{and } \nabla\nabla^T u_3^P(x) &= D^2(u^M,\theta)(x) + \overline{\mathcal{L}^B D^2(u^M,\theta)}(x,\frac{x}{\varepsilon}) + O(\varepsilon) \end{aligned} \tag{16}$$

whereas in ω_C, it follows that

$$\begin{aligned} u_3^P(x) &= u^M(x) + \overline{u^C}(x,\frac{x}{\varepsilon}) + O(\varepsilon), \\ \varepsilon\nabla u_3^P(x) &= \overline{\nabla_y u^C}(x,\frac{x}{\varepsilon}) + O(\varepsilon) \text{ and } \varepsilon^2\nabla\nabla^T u_3^P(x) = \overline{\nabla_y \nabla_y^T u^C}(x,\frac{x}{\varepsilon}) + O(\varepsilon) \end{aligned} \tag{17}$$

where ∇_y is the gradient with respect to y,

$$D(u^M,\theta)=\begin{pmatrix}\partial_{x_1}u^M\\ \theta\end{pmatrix} \text{ and } D^2(u^M,\theta)=\begin{pmatrix}\partial^2_{x_1x_1}u^M & \partial_{x_1}\theta\\ \partial_{x_1}\theta & 0\end{pmatrix}$$

and $\overline{v}$ is defined in (54). The construction of (u^M,θ), of the fourth order tensor $\mathcal{L}^B$ and of u^C is done as follows. First, one builds $\mathcal{L}^B$ so that

$$(\nabla_y\nabla_y^T w^B)_{\alpha\beta}=\sum_{\gamma,\rho=1}^{2}\mathcal{L}^B_{\alpha\beta\gamma\rho}\begin{pmatrix}\nu & \mu\\ \mu & 0\end{pmatrix}_{\gamma\rho} \tag{18}$$

where w^B is solution of the microscopic problem $\mathcal{P}_B$ posed in the base Y_B. Once this is done, the calculation of (u^M,θ) is made possible by solving the problem macro $\mathcal{P}^M$ related to the macroscopic domain ω and the base Y_B. Finally, u^M being known, u^C may be computed due to the microscopic problem $\mathcal{P}^C$ posed in Y_C. We note that in the case of atomic forces depending on u^C, the macroscopic problem $\mathcal{P}^M$ and the microscopic problem $\mathcal{P}^C$ in the cantilever cannot be solved sequentially since they are fully coupled through the expression of the atomic forces when its action on the tip has a non negligible effect on the base's solution (u^M,θ).

Problem $\mathcal{P}^M$: The set of edges of the macroscopic domain ω where $x_1=0$ or 1 splits in γ_0^M and γ_1^M corresponding, respectively, to the area where the base is clamped and where it is free. The statement of the macroscopic or homogenized problem $\mathcal{P}^M$ includes the equilibrium equations

$$\partial^2_{x_1x_1}M_1^M=f_1^M \text{ and } \partial_{x_1}M_2^M=f_2^M \text{ in } \omega \tag{19}$$

and the stress-strains relation

$$M_1^M=R_{11}^M\partial^2_{x_1x_1}u^M+R_{12}^M\partial_{x_1}\theta,\ M_2^M=R_{21}^M\partial^2_{x_1x_1}u^M+R_{22}^M\partial_{x_1}\theta \text{ in } \omega \tag{20}$$

along with the boundary conditions

$$\begin{aligned} u^M &= \partial_{x_1}u^M=\theta=0 \text{ on } \gamma_0^M \\ \text{and } M_1^M &= M_2^M=0,\ \partial_{x_1}M_1^M=g^M \text{ on } \gamma_1^M. \end{aligned} \tag{21}$$

The new parameters are

$$g^M=\int_{Y_B}g_1^B\ dy,\ f_1^M=\int_Y f^0\ dy+\int_{Y_B}\partial_{x_1}g_1^B\ dy,\ f_2^M=\int_{Y_B}g_2^B\ dy$$

$$R^M=\begin{pmatrix}\widetilde{R}^M_{1111} & 2\widetilde{R}^M_{1211}\\ 2\widetilde{R}^M_{1211} & 4\widetilde{R}^M_{1212}\end{pmatrix}$$

where the fourth order tensor $\widetilde{R}^M$ is defined by

$$\widetilde{R}^M_{\alpha\beta\gamma\rho}=\int_{Y_B}R^B_{\alpha\beta\gamma\rho}+R^B_{\alpha\beta\xi\zeta}\mathcal{L}^B_{\xi\zeta\gamma\rho}\ dy,$$

$\mathcal{L}^B$ is defined by (18) and w^B is solution of the problem $\mathcal{P}^B$.

The variational formulation is

$$(u^M,\theta)\in V^M,\ \int_\omega M^M.(\partial^2_{x_1x_1}v,\partial_{x_1}\eta)^T\ dx=\int_\omega f_1^Mv-g^M.D(v,\eta)\ dx \text{ for all } (v,\eta)\in V^M \tag{22}$$

where

$$V^M = \{(v,\eta) \in L^2(\omega)^2 \ / \ \partial^2_{x_1x_1} v \text{ and } \partial_{x_1}\theta \in L^2(\omega),\ v = \partial_{x_1} v = \theta = 0 \text{ on } \gamma_0^M\},$$

$L^2(\omega)$ being the set of square integrable functions on ω.

Problem $\mathcal{P}^B$: The boundary of Y_B is made up of the interface $\gamma_{B,F}$ between Y_B and Y_F, the area γ_{per} corresponding to the junction between neighboring cells and the remaining part γ_{B1}. The microscopic equations stated in the base Y_B are

$$div_y(div_y(M^B)) = -div_y(div_y(F^B)) \text{ with } M^B = R^B \nabla_y \nabla_y^T w^B \text{ and } F^B = R^B \begin{pmatrix} \nu & \alpha \\ \alpha & 0 \end{pmatrix}. \quad (23)$$

The boundary conditions are

$$\begin{aligned} \nabla_y(n_y^T M^B \tau_y).\tau_y + div_y(M^B).n_y &= -\nabla_y(n_y^T F^B \tau_y).\tau_y - div_y(F^B).n_y \\ \text{and } n_y^T M^B n_y &= -n_y^T F^B n_y \text{ on } \gamma_{B1} \cup \gamma_{B,F} \end{aligned}$$

and

$$w^B,\ n_y^T M^B n_y,\ \nabla w^B.n,\ \nabla_y(n_y^T M^B \tau_y).\tau_y + div_y(M^B).n_y \text{ are } Y-\text{periodic on } \gamma_{per}.$$

Finally, w^B and $\nabla_y w^B$ are set equal to zero in an arbitrary point y^0 of Y_B so that to garantee the uniqueness. The variational formulation is

$$u^B \in V^B,\ \int_{Y_B} M^B :: \nabla_y \nabla_y^T v \ dy = -\int_{Y_B} F^B \nabla_y \nabla_y^T v \ dx \text{ for all } v \in V^B \quad (24)$$

where

$$V^B = \{v \in H^2(Y_B) \ / \ v,\ \nabla_y v \text{ are } Y-\text{periodic on } \gamma_{per}\}.$$

We note that the solution of this variational formulation is unique up to a function v such that $\nabla_y \nabla_y^T v = 0$ and v, $\nabla_y v$ are $Y-$periodic on γ_{per}, in short up to a function $v(y) = a_0 + a_1 y_2$.

Problem $\mathcal{P}^C$. The boundary of the elastic part Y_F of the cantilever is the union of the interface $\gamma_{B,F}$ between the base and the cantilever, the interface $\gamma_{B,R}$ between the elastic part and the rigid part and the remaining γ_{F1}. The data $\widehat{f^P}$ and g^C being given, the problem $\mathcal{P}^C$ used for the calculation of u^C is made up of the equilibrium equations, the stress-strains relation and the rigidity constraint

$$\begin{aligned} div_y(div_y(M^C)) = f^0 + div_y g^C \text{ and } M^C = R^C \nabla_y \nabla_y^T u^C \text{ in } Y_F, \\ u^C = b^C + B^C.y \text{ in } Y_R, \end{aligned} \quad (25)$$

the boundary conditions

$$\begin{aligned} u^C &= \nabla_y u^C.n_y = 0 \text{ on } \gamma_{B,F}, \\ n_y^T M^C n_y &= 0,\ \nabla_y(n_y^T M^C \tau_y).\tau_y + div_y(M^C).n_y = 0 \text{ on } \gamma_{F1}, \end{aligned}$$

the continuity of u^C and $\nabla_y u^C$ through the interface $\gamma_{F,R}$ and the normal stresses transmission

$$b^C = |\gamma_{F,R}|^{-1} \int_{\gamma_{F,R}} (u^C - \nabla u^C.x)_{|Y_F} \ ds,\ B^C = |\gamma_{F,R}|^{-1} \int_{\gamma_{F,R}} (\nabla u^C)_{|Y_F} \ ds$$

$$-\int_{\gamma_{F,R}} div_y(M^C).n_y \ ds = \xi^C,\ \int_{\gamma_{F,R}} n_y^T M^C - (div_y(M^C).n_y) y \ ds = \Xi^C$$

where

$$\xi^C = \int_{Y_R} f^0 \, dy - \int_{\gamma_{F,R}} (g^C.n_y)_{|Y_F} \, ds \text{ and } \Xi^C = \int_{\gamma_{F,R}} -(g^C.n_y)_{|Y_F} y \, ds + \int_{Y_R} f^0 \, y - g^C \, dy. \tag{26}$$

The corresponding variational formulation is

$$u^C \in V^C, \ \int_{Y_F} M^C :: \nabla_y \nabla_y^T v \, dy = \int_{Y_C} f^0 v - g^C.\nabla_y v \, dy \text{ for all } v \in V^C \tag{27}$$

where

$$V^C = \{v \in H^2(Y_C) \ / \ v = \nabla_y v.n_y = 0 \text{ on } \gamma_{B,F}, \ \nabla_y \nabla_y^T v = 0 \text{ in } Y_R\}.$$

4.2 Derivation of the Two-scale Model

The proof follows three steps. First a specific estimate of the growth of the mechanical displacement is derived with respect to the small parameter ε. In a second step we use the Taylor expansion of the two scale transform of u^P and identify the global system which is verified by the coefficients of the Taylor expansion. It is from this global system that the wanted model is extracted.

The mathematical formulation of the assumptions on the rigidity and on the external forces is in the one side an uniform ellipticity condition: there exists a constant K such that for all $\varepsilon > 0$ and all 2×2 symmetric matrix ξ,

$$[R^B \xi] :: \xi \text{ and } [R^C \xi] :: \xi \geq K|\xi|^2$$

and in the other side there exists another constant C such that for all $\varepsilon > 0$,

$$||\widehat{f}^P||_{\omega_P \times Y} + ||\widehat{g}^P||_{\omega_P \times Y_B} + ||g^C||_{\omega_P \times Y_C} \leq C.$$

In the proof, for the sake of simplicity, we remove the uperscript of u_3^P, f^P and g^P.

(i) Let us prove the estimates

$$||u||_{\omega_P}, \ ||\nabla u||_{\omega_B}, \ ||\varepsilon \nabla u||_{\omega_C}, \ ||\nabla \nabla^T u||_{\omega_B}, \ ||\varepsilon^2 \nabla \nabla^T u||_{\omega_C} \leq C \tag{28}$$

uniformly with respect to ε. One starts from the variational formulation (13) where one equales $v = u$

$$\begin{aligned} & \int_{\omega_B} [R^P \nabla \nabla^T u] :: \nabla \nabla^T u \, dx + \int_{\omega_F} \varepsilon^{-4} [R^P (\varepsilon^2 \nabla \nabla^T u)] :: (\varepsilon^2 \nabla \nabla^T u) \, dx \\ = & \int_{\omega_P} f.u - \chi_{\omega_B} g.\nabla u - \chi_{\omega_C} \varepsilon^{-1} g.(\varepsilon \nabla u) \, dx, \end{aligned}$$

one applies the uniform ellipticity condition and use the fact that $\nabla \nabla^T u = 0$ in ω_R,

$$X = K(||\nabla \nabla^T u||_{\omega_B}^2 + ||\varepsilon^2 \nabla \nabla^T u||_{\omega_C}^2) \leq ||f||_{\omega_P} ||u||_{\omega_P} + ||(\chi_{\omega_B} + \varepsilon^{-1} \chi_{\omega_C}) g||_{\omega_P} ||(\chi_{\omega_B} + \varepsilon \chi_{\omega_C}) \nabla u||_{\omega_P},$$

and then the estimates on the external forces

$$X \leq C_1(||u||_{\omega_P} + ||(\chi_{\omega_B} + \varepsilon \chi_{\omega_C}) \nabla u||_{\omega_P}).$$

Thanks to the Poincaré like estimate (66),

$$X \leq C_2||(\chi_{\omega_B} + \varepsilon^2 \chi_{\omega_C})\nabla\nabla^T u||_{\omega_P}.$$

The third estimate in (28) follows and the two others are a direct consequence of it and of (66).

(ii) Let us establish that (u^M, θ, u^B, u^C) is solution of the two-scale variational formulation:

$$(u^M, \theta, u^B, u^C) \in \mathcal{V},\ \int_{\omega\times Y_B} M :: [D^2(v^M, \eta) + \nabla_y \nabla_y^T v^B]\ dydx + \int_{\omega\times Y_F} M^C :: \nabla_y \nabla_y^T v^C\ dydx = \tag{30}$$

$$\int_{\omega\times Y_P} f^0.v^M\ dydx - \int_{\omega\times Y_B} g^B.D(v^M, \eta)\ dydx - \int_{\omega\times Y_C} g^C.\nabla_y v^C\ dydx + O(\varepsilon)$$

for all $(v^M, \eta, v^B, v^C) \in \mathcal{V}$ with

$$M = R^B(D^2(u^M, \theta) + \nabla_y \nabla_y^T u^B),\ M^C = R^C \nabla_y \nabla_y^T u^C$$

and

$$\mathcal{V} = \mathcal{V}^M \times L^2(\omega; V^B) \times L^2(\omega; V^C)$$

where

$$\mathcal{V}^M = \{(v^M, \eta) \in H^2(\omega) \times H^1(\omega)\ /\ v^M = \nabla v^M.n = \theta = 0 \text{ on } \gamma_0^M\}.$$

We assume that u can be expanded as $\widehat{u} = u^0 + \varepsilon u^1 + \varepsilon^2 u^2 + \varepsilon^2 O(\varepsilon)$ which is partially justified by (28). We make use of the results stated in the appendix for $\omega_1 = \omega_P$ and thus $d = 2$. The domain ω_P is clearly not connected in the direction x_2 parallel to the cantilevers and connected in the direction x_1 parallel to the base.

Let us make the link between the general notation used in the appendix and the specific notations of the two-scale model presented in this paper. We pose

$$\begin{aligned} u^M &= u^0_{|\omega\times Y_B},\ \theta = \partial_{y_2} u^1 \text{ and } u^B = u^2 \text{ in } \omega \times Y_B, \\ u^C &= u^0 - u^M \text{ in } \omega \times Y_C. \end{aligned}$$

Thus $(u^M, \theta, u^B, u^C) \in \mathcal{V}$ and

$$(\widehat{u}, \widehat{\nabla u}, \widehat{\nabla\nabla^T u}) = (u^M, D(u^M, \theta), D^2(u^M, \theta) + \nabla_y \nabla_y^T u^B) + O(\varepsilon) \text{ in } \omega \times Y_B, \tag{31}$$

$$\text{and } (\widehat{u}, \varepsilon\widehat{\nabla u}, \varepsilon^2\widehat{\nabla\nabla^T u}) = (u^M + u^C, \nabla_y u^C, \nabla_y \nabla_y^T u^C) + O(\varepsilon) \text{ in } \omega \times Y_C$$

where the approximations are in the weak sense as defined in appendix. Now consider the test functions $(v^M, \eta, v^B, v^C) \in \mathcal{V}$ and v^1 such that $\partial_{y_2} v^1 = \eta$. Let us pose

$$v = v^M + \varepsilon v^1 + \varepsilon^2 v^B \text{ in } \omega \times Y_B \text{ and } v = v^M + v^C \text{ in } \omega \times Y_C.$$

We restrict to regular functions v^1 and v^2 such that $\overline{v}^1$ satisfies the boundary conditions so that they belong to V^P. Then according to the definition (54), it appears that $\overline{v}(x, \frac{x}{\varepsilon}) \in V^P$ and it may be chosen as a test function in the variational formulation (13) that we rewrite:

$$\begin{aligned} u \in V^P,\ &\int_{\omega_B} M^P :: \nabla\nabla^T \overline{v}\ dx + \int_{\omega_F} M^{P1} :: (\varepsilon^2 \nabla\nabla^T \overline{v})\ dx \\ = &\int_\omega f.\overline{v}\ dx - \int_{\omega_B} g.\nabla\overline{v}\ dx - \int_{\omega_C} (\varepsilon^{-1} g).(\varepsilon\nabla\overline{v})\ dx \end{aligned} \tag{32}$$

with

$$M^{P1} = (\varepsilon^{-4} R^P)(\varepsilon^2 \nabla \nabla^T u).$$

Let us focus our attention to the first integral. We remark that

$$\nabla \nabla^T \overline{v} = (D^2(\overline{v}^M, \eta) + \nabla_y \nabla_y^T \overline{v}^B)(x, \frac{x}{\varepsilon}) + O(\varepsilon) \text{ in } \omega_B$$

From (56) it is also approximated by $T^*(E_{Y_B}(D^2(v^M, \eta) + \nabla_y \nabla_y^T v^B))(x) + O(\varepsilon)$ so

$$X = \int_{\omega_B} M^P :: \nabla \nabla^T \overline{v} \; dx = \int_{\omega} E_{\omega_B} M^P :: T^*(E_{Y_B}(D^2(v^M, \eta) + \nabla_y \nabla_y^T v^B)) \; dx + O(\varepsilon)$$

because $||M^P||_{\omega_B}$ is bounded. Here E_{ω_B} and E_{Y_B} denote the operators that extend by 0 a function defined on ω_B or Y_B to a function defined in ω or Y. Let us rewrite it by transposing T^*:

$$X = \int_{\omega \times Y} \widehat{E_{\omega_B} M^P} :: E_{Y_B}(D^2(v^M, \eta) + \nabla_y \nabla_y^T v^B) \; dx + O(\varepsilon).$$

Using the identity $T(E_{\omega_B} M^P) = E_{Y_B} R^B \widehat{\nabla \nabla^T u}$ and the approximation of $\widehat{\nabla \nabla^T u}$ yields

$$X = \int_{\omega \times Y_B} [R^B(D^2(u^M, \theta) + \nabla_y \nabla_y^T u^B)] :: (D^2(v^M, \eta) + \nabla_y \nabla_y^T v^B) \; dx + O(\varepsilon)$$

which is the first term of (30). The same procedure applied to each terms of (32), provided that

$$\begin{aligned} \nabla \overline{v} &= D(v^{M*}, \eta)(x, \frac{x}{\varepsilon}) + O(\varepsilon) \text{ in } \omega_B \\ \text{and } \varepsilon \nabla \overline{v} &= \nabla_y \overline{v}^C(x, \frac{x}{\varepsilon}) + O(\varepsilon), \varepsilon^2 \nabla \nabla^T \overline{v} = \nabla_y \nabla_y^T \overline{v}^C(x, \frac{x}{\varepsilon}) + O(\varepsilon) \text{ in } \omega_C, \end{aligned}$$

leads to the complete formulation (30).

(iii) From the two-scale variational formulation, we now derive successively the three problems $\mathcal{P}^B$, $\mathcal{P}^C$ and $\mathcal{P}^M$.

For the derivation of $\mathcal{P}^B$ one starts by choosing $\eta = v^M = v^C = 0$ and remark that

$$M^M = R^B D^2(u^M, \theta) + M^B$$

then

$$\int_{\omega \times Y_B} M^B :: \nabla_y \nabla_y^T v^B \; dydx = \int_{\omega \times Y_B} -[R^B D^2(u^M, \theta)] :: \nabla_y \nabla_y^T v^B \; dydx.$$

Making the choice $v^B(x, y) = \varphi(x) \widetilde{v}^B(y)$ with any regular φ vanishing on the boundary of ω allows us to eliminate the integrals over ω and yields the variational formulation (23) where we have removed the $O(\varepsilon)$ term.

For the derivation of $\mathcal{P}^C$ one poses $\eta = v^M = v^B = 0$ which leads to

$$\int_{\omega \times Y_F} M^C :: \nabla_y \nabla_y^T v^C \; dydx = \int_{\omega \times Y_C} \widehat{f}.v^M - g^C.\nabla_y v^M \; dydx.$$

Based on the same argument, the integrals over ω may be removed and (25) follows.

Finally one derives $\mathcal{P}^M$ by posing $v^B = v^C = 0$ and using the fact that

$$\nabla_y \nabla_y^T u^B = \mathcal{L}^B D^2(u^M, \theta). \tag{33}$$

It follows that

$$\int_\omega M^M :: D^2(v^M, \eta)\ dydx = \int_{\omega \times Y_P} \widehat{f}.v^M\ dydx - \int_{\omega \times Y_B} \widehat{g}.D(v^M, \eta)\ dydx$$

and the variational formulation (22) follows. The final approximation of u^P and of their derivatives comes from the application of T^* to (31) plus the linear relation (33) and finally the general approximation $T^* v(x) = \overline{v}(x, \dfrac{x}{\varepsilon})$.

5 Tip Forces

To characterize the behavior of the cantilever, it is necessary to quantify the attractive forces F^{vdW} of van der Waals type and repulsive forces F^{rep} between the tip and sample. We consider first the development of relations for F^{vdW}.

As detailed in [28, 21], attractive forces result primarily from van der Waals forces that are due to a combination of electrostatic and dispersional effects present between all atoms and molecules. Either classical or quantum principles can be used to derive the van der Waals potential

$$W^{vdW}(\zeta) = -\frac{C}{||\zeta||^6} \text{ where } \zeta = x' - x \tag{34}$$

for two atoms or molecules located respectively at the positions x and x'. Here $||\zeta|| = (\zeta_1^2 + \zeta_2^2 + \zeta_3^2)^{1/2}$ and $C = \frac{\alpha_0^2 \hbar \nu}{(4\pi\varepsilon_0)^2}$ is a constant which depends on the electronic polarizability α_0 of constituent atoms, Planck's constant $\hbar$, the electron orbital frequency ν, and the permittivity ε_0 of vacuum.

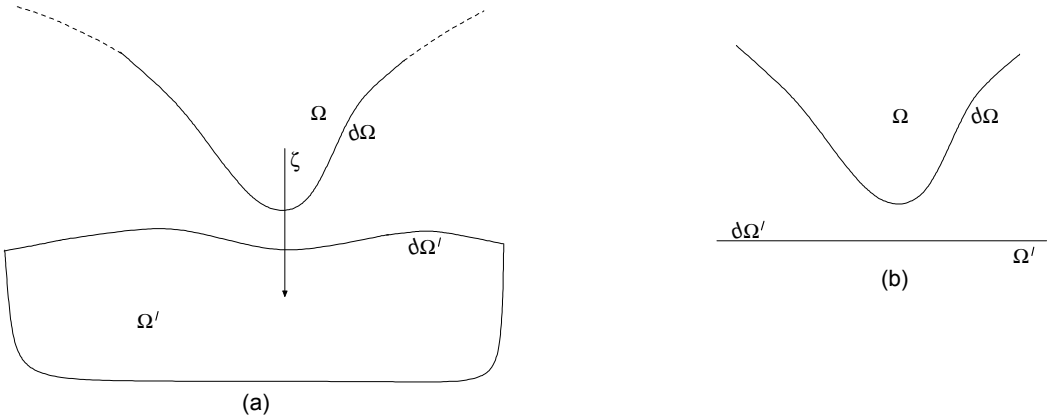

Figure 3: Geometry of the AFM tip and sample with the assumption of (a) general surfaces, and (b) a locally flat sample

To construct macroscopic relations quantifying the force between the cantilever tip and sample, we consider first the general case in which the tip and sample are arbitrary bodies Ω and Ω' having densities ρ and ρ'.

To determine the force, we make the classical assumptions of Hamaker which can be summarized as (i) additivity of individual atomic or molecular contributions, (ii) continuous media

so that summation can be replaced by integration, and (iii) constant material properties. For these assumptions, the force exerted by the particule located in x' on this in x is given by

$$F^{vdW} = \rho\rho' \int_{\Omega} \int_{\Omega'} f(x' - x)\ dxdx' \tag{35}$$

where $f = -\nabla W$.

The determination of F for arbitrary geometries and potential W necessitates approximation of integrals over six dimensions which is typically prohibitive. To simplify the formulation, we follow the approach of [26, 27] and reformulate the relation in terms of surface integrals. We consider the vector field

$$G = \frac{-C\zeta}{3||\zeta||^6}. \tag{36}$$

It follows that

$$divG = -W \tag{37}$$

and hence the divergence theorem can be invoked to formulate the macroscopic force as

$$F^{vdW} = \rho\rho' \int_{\partial\Omega} \int_{\partial\Omega'} (G.n')n\ ds'ds \tag{38}$$

where n and n' respectively denote normals to the tip and sample. For the vector field relation (36), the force is

$$F^{vdW} = -\frac{A}{3\pi^2} \int_{\partial\Omega} \int_{\partial\Omega'} \frac{\zeta.n'}{||\zeta||^6} n\ ds'ds \tag{39}$$

where the Hamaker constant is

$$A = \pi^2 C\rho\rho'. \tag{40}$$

The flat sample case: For various applications, it is reasonable to approximate the sample by a locally flat surface (n' constant) while retaining the general representation for the cantilever tip, see Figure 3 (b). For example, this assumption is reasonable when identifying the tip shape using a known sample with minimal curvature or for regimes in which the separation distance is large compared with perturbations in the sample. From the approximation

$$\int_{\partial\Omega'} \frac{\zeta.n'}{||\zeta||^6} n\ ds \approx \int_{\mathbb{R}^2} \frac{\zeta.n'}{||\zeta||^6}\ dx'_1 dx'_2 = \int_{\mathbb{R}^2} \frac{\zeta.n'}{||\zeta||^6}\ d\zeta_1 d\zeta_2 = \frac{\pi}{2(\zeta.n')^3}.$$

the attractive force is

$$F^{vdW} = \frac{A}{6\pi} \int_{\partial\Omega} \frac{n}{(\zeta.n')^3}\ ds. \tag{41}$$

The simplified force relation (41) facilitates implementation when identifying the tip shape or operating in regimes in which the separation distance is sufficiently large so that modulations in the sample surface are negligible.

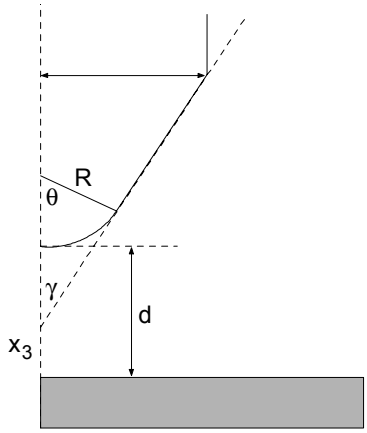

Figure 4: Geometry of the AFM tip

Flat sample and parameterized tip: Finally, we consider the case in which the sample surface is assumed locally flat and a simple geometric parameterization is assumed for the cantilever tip. Specifically, we follow the approach of Argento and French [26] and assume that the cantilever can be parameterized as having a spherical tip of radius R, and a conical section as depicted in Figure 3 with a distance d from the sample. This geometry is motivated by scanning electron microscopy (SEM) images of various AFM tips and provides sufficient flexibility for a number of applications while limiting to commonly employed models for spherical probes.

This assumption allows cylindrical symmetry to be invoked to yield analytic force relations, and relaxation of this assumption would necessitate the approximation of nonsymmetric contributions which yield higher-order force effects.

As detailed in [26], the attractive force due to van der Waals interactions can in this case be expressed as

$$F^{vdW}(d) = \frac{AR^2[1-\sin\gamma][R\sin\gamma - d\sin\gamma - R - d]}{6d^2[R+d-R\sin\gamma]^2} - \frac{A\tan\gamma[d\sin\gamma + R\sin\gamma + R\cos(2\gamma)]}{6\cos\gamma[d+R-R\sin\gamma]^2} \tag{42}$$

where A is the Hamaker constant specified in (40) and γ is the cone angle shown in Figure 3.

The repulsive forces are due to the overlap of electron clouds. These are quantum mechanical in nature and very short range compared with the attractive forces. Phenomenological arguments yield microscopic potential relations of the form

$$W^{rep}(\zeta) = \frac{B}{||\zeta||^{12}} \tag{43}$$

where B is a constant which depends on electronic and material properties of the sample and tip. Arguments analogous to those for the attractive forces yield short-range force relations analogous to (39), (**??**), or (42).

6 Examples

An example illustrating the application of the thin plate model for an AFM is presented in Section 6.1. In Section 6.2, the two-scale model is applied to an AFM array. Finally in Section 6.3, results for a simulation of the AFM array are reported and discussed.

6.1 A Single AFM

The two-dimensional domain ω_P is a rectangle $\omega_P = (0, \ell_C^0) \times (0, L_C)$ with $\ell_C^0 << L_C$. The plate is made up of an homogeneous isotropic material, is clamped on the side $x_1 = 0$ and is left free otherwhere. The elastic part is $\omega_E = (0, \ell_C^0) \times (0, L_E)$ and the rigid part is its complementary set $\omega_R = (0, \ell_C^0) \times (L_E, L_C)$. The coordinates of the tip are $x^{tip} = (x_1^{tip}, x_2^{tip}, x_3^{tip})$. The shape of the sample to be analyzed is parameterized by a function $\phi(x_1, x_2)$. The force applied on the tip is modelled as a concentrated force

$$f_1 = f_2 = 0 \text{ and } f_3(x) = F(d)\delta_{x^{tip}}(x)$$

where $d = u^{tip} - \phi^{tip}$with $\phi^{tip} = \phi(x_1^{tip}, x_2^{tip})$ and $u^{tip} = u(x^{tip})$. Let us denote by x^G the gravity center of Ω_R and assume that $x^{tip} - x^G$ is parallel to the direction of x_3. If the dependency of u_3^P with respect to x_1 is neglected, then the distance d between the tip and the sample is the unique solution of the nonlinear algebraic equation

$$k^P(x_2^{tip})(d + \phi^{tip}) - F(d) = 0 \tag{44}$$

and when d is known u_3^P is computed by

$$u_3^P(x_2) = F(d)/k^P(x_2) \text{ for } x_2 \in [0, L_C]$$

where

$$\begin{aligned} k^P(x_2) &= \frac{6m^P}{x_2^2(3H^P|\omega_R|/|\Omega_R| - x_2)} \text{ in } [0, L_E] \\ &= \frac{6|\Omega_R|m^P}{L_E(-3L_E H^P|\omega_R| + 2L_E^2|\Omega_R| + 6x_2 H^P|\omega_R| - 3x_2 L_E|\Omega_R|)} \text{ in } (L_E, L_C], \end{aligned}$$

and

$$\begin{aligned} m^P &= \frac{8\mu a^3(\lambda + \mu)\ell_C^0}{3(\lambda + 2\mu)}, \\ h^P = |\omega_R|^{-1}|\Omega_R|,\ H^P &= |\omega_R|^{-1} \int_{\omega_R} (a + h(x))x_2 \, dx. \end{aligned} \tag{45}$$

The proof is straightforward and we mention only the main steps. From Section 7.4,

$$f^P(x) = \frac{a + h(x)}{|\Omega_R|} F(d) \text{ in } \omega_R,\ f^P = 0 \text{ in } \omega_E,\ g^P = 0 \text{ in } \omega_P,$$

thus

$$\xi^P = \int_{\omega_R} \frac{a + h(x)}{|\Omega_R|} \, dx \ F = F \text{ and } \Xi_2^P = \frac{H^P|\omega_R|}{|\Omega_R|} F.$$

The displacement u_3^P is solution of the boundary value problem

$$\begin{aligned} \frac{d^4 u_3^P}{dx_2^4}(x_2) &= 0 \text{ for } x_2 \in (0, L_E),\ u_3^P(0) = \frac{du_3^P}{dx_2}(0) = 0 \\ -m^P \frac{d^3 u_3^P}{dx_2^3}(L_E) &= \xi^P \text{ and } m^P(\frac{d^2 u_3^P}{dx_2^2} - \frac{d^3 u_3^P}{dx_2^3} x_2)(L_E) = \Xi_2^P \end{aligned} \tag{46}$$

where $m^P = \ell_C^0 R_{2222}^P$. In the rigid part

$$u_3^P(x_2) = b^P + B_2^P x_2$$

with

$$b^P = u_3^P(L_E) - \frac{du_3^P}{dx_2}(L_E)L_E \text{ and } B_2^P = \frac{du_3^P}{dx_2}(L_E).$$

In particular,

$$u^{tip} = b^P + B_2^P x_2^{tip}.$$

The equations (46) yield $u_3^P(x_2) = a_0 + a_1 x_2 + a_2 x_2^2 + a_3 x_2^3$ in the elastic part with

$$a_0 = a_1 = 0,\ 2m^P a_2 = \Xi_2^P \text{ and } -6m^P a_3 = \xi^P \tag{47}$$

from which the equation $u_3^P(x_2) = F(d)/k^P(x_2)$ follows. The equation of d follows by taking $x_2 = x_2^{tip}$ and using the relation $u_3^P(x_2^{tip}) = d + \phi^{tip}$.

6.2 An AFM Array

The whole system is still comprised of a homogeneous isotropic material. The subdomains Y_B and Y_C are two rectangles described respectively in the coordinates (O_B, y_1^B, y_2^B) and (O_C, y_1^C, y_2^C) by

$$Y_B = (0,1) \times (0, \ell_B) \text{ and } Y_C = (0, \ell_C^0) \times (0, L_C)$$

where $O_C = (-\frac{\ell_C^0}{2}, \ell_B - \frac{1}{2})$, $O_B = (-\frac{1}{2}, -\frac{1}{2})$, $y^B = y - O_B$ and $y^C = y - O_C$, see Figure 5 for the description of the cell and Figure 4 for the changes of coordinates. The flexible part Y_F of Y_C is $(0, \ell_C^0) \times (0, L_F)$ in (O_C, y^C).

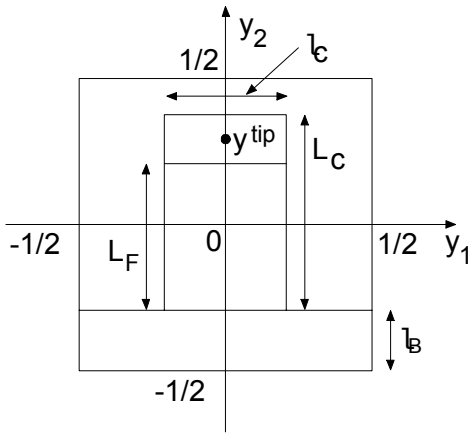

Figure 5: Reference cell

We assume that $\gamma_1^M = \varnothing$ so $\gamma_0^M = \{0,1\} \times (0,1)$. The tip coordinates are denoted by y^{tip} in (O, y_1, y_2), by y^{Ctip} in (O_C, y_1^C, y_2^C) and by $x_i^{tip} = (x_{i1}^{tip}, x_{i2}^{tip}, x_{i3}^{tip})$ in Ω.

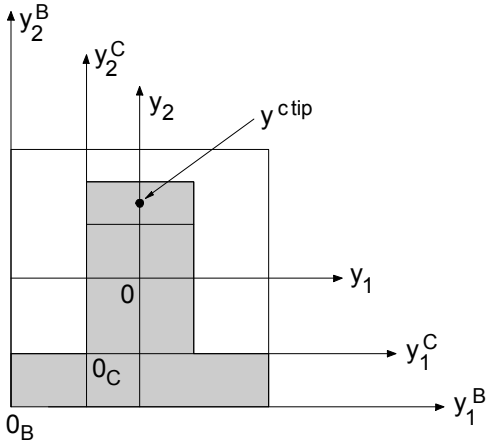

Figure 6: Local coordinates in Y_B and Y_C

The force applied to the cantilever is assumed to be concentrated on each tip, so that

$$f_1 = f_2 = 0 \text{ and } f_3(x) = \sum_i F(u_3(x_i^{tip}) - \phi(x_{1i}^{tip}, x_{2i}^{tip}))\delta_{x_i^{tip}}(x) \text{ in } \Omega.$$

The corresponding volumic force can be computed by using the results of Section 7.4. We assume that it satisfies the assumptions done for the derivation of the two-scale model. Then for $d(x) = u^M(x) + u^C(x, y^{Ctip}) - \phi(x)$, the model is stated as follows. The couple (d, u^M) is solution of

$$\begin{gathered} R_{11}^M \partial^4_{x_1x_1x_1x_1} u^M(x) = F(d(x))/\varepsilon \text{ for all } x \in \omega \\ u^M(0,x_2) = u^M(1,x_2) = \partial_{x_1} u^M(0,x_2) = \partial_{x_1} u^M(1,x_2) = 0 \text{ for all } x_2 \in (0,L_2) \end{gathered} \tag{48}$$

and

$$k^C(y_2^{Ctip})(d + \phi - u^M)(x) - F(d(x))/\varepsilon = 0 \text{ for all } x \in \omega. \tag{49}$$

Once d is known, u^C is computed by

$$k^C(y_2^C)u^C(x,y_2) = F(d(x))/\varepsilon \text{ for all } (x, y_2^C) \in \omega \times (0, L_C)$$

where

$$\begin{aligned} k^C(y_2) &= \frac{6m^C}{y_2^2(3H^C|Y_R|/|V_R| - y_2)} \text{ in } [0, L_F] \\ &= \frac{6|V_R|m^C}{L_F(-3L_FH^C|Y_R| + 2L_F^2|V_R| + 6y_2H^C|Y_R| - 3y_2L_F|V_R|)} \text{ in } (L_F, L_C], \end{aligned}$$

$$H^C = |Y_R|^{-1} \int_{Y_R} (a^C + h^0(y))y_2 \, dy, \; h^0(y) = h(x_i + \varepsilon y)/\varepsilon,$$

$$R_{11}^M = \frac{4\mu a_B^3 \ell_B \varepsilon^4}{3(\lambda + 2\mu)}(2\lambda + 2\mu - \frac{\lambda^2}{2(\lambda+\mu)}), \; m^C = \frac{8\mu a_C^3(\lambda+\mu)\ell_C^0}{3(\lambda+2\mu)}.$$

Moreover, $\mathcal{L}^B(\nabla\nabla^T u^M) = -\dfrac{2\lambda}{4(\lambda+\mu)} \begin{pmatrix} 0 & 0 \\ 0 & 1 \end{pmatrix}$ and $\theta = 0$. Remark that h^C and H^C are independent of the cell center x_i because h is periodic. Here we have used the notations a_B

and a_C for the thickness of the base and of the cantilever divided by ε and $V_R \subset \mathbb{R}^3$ the three-dimensional dilatation of any of the tips in Ω_R.

Let us sketch the derivation. From Section 7.4, the surface force in the thin plate model is

$$f^P(x) = \sum_i \frac{a_C + h^0((x-x_i)/\varepsilon)}{|V_R|} F(u^P(x_i^{tip}) - \phi(x_i^{tip}))\chi_{Y_i}(x)$$

where $x_i^{tip} = (x_{i1}^{tip}, x_{i2}^{tip})$ and u^P stands for the approximation of u_3. Its two-scale transform is

$$\widehat{f}^P(x,y) = \frac{a_C + h^0(y)}{|V_R|} F(\widehat{u}^P(x, y^{tip}) - \widehat{\phi}(x, y^{tip}))/\varepsilon^2$$

then

$$f^0(x,y) = \frac{a_C + h^0(y)}{|V_R|} F(u^M(x) + u^C(x, y^{tip}) - \phi(x))/\varepsilon^2.$$

From that expression, one may derive the solutions of the three problems $\mathcal{P}^B$, $\mathcal{P}^M$ and $\mathcal{P}^C$.

Problem $\mathcal{P}^B$: The solution w^B of $\mathcal{P}^B$ is

$$w^B(y^B) = -\frac{\lambda\nu}{4(\lambda+\mu)}(y_1^B)^2.$$

This is verified by showing that such w^B satisfies the variational formulation. Thus

$$M^B = \frac{8\mu K}{3(\lambda+2\mu)} \begin{pmatrix} \lambda & 0 \\ 0 & 2(\lambda+2\mu) \end{pmatrix} \text{ with } K = -\frac{\lambda\nu}{4(\lambda+\mu)}$$

and

$$\int_{Y_B} M^B \nabla_y \nabla_y^T v \; dy = \frac{16\mu(\lambda+\mu)K}{3(\lambda+2\mu)} \int_{Y_B} \partial^2_{y_1 y_1} v \; dy$$

because $\int_{Y_B} \partial^2_{y_2 y_2} v \; dy = 0$ due to the periodicity of $\partial_{y_1} v$ on γ_{per}. By another way,

$$F^B = \frac{4\mu}{3}\left(\frac{\nu}{\lambda+2\mu} \begin{pmatrix} 2(\lambda+\mu) & 0 \\ 0 & \lambda \end{pmatrix} + \begin{pmatrix} 0 & \alpha \\ \alpha & 0 \end{pmatrix}\right)$$

then

$$\int_{Y_B} F^B \nabla_y \nabla_y^T v \; dy = \frac{4\mu\lambda\nu}{3(\lambda+2\mu)} \int_{Y_B} \partial^2_{y_2 y_2} v \; dy$$

because $\int_{Y_B} \partial^2_{y_1 y_1} v \; dy = \int_{Y_B} \partial^2_{y_1 y_2} v \; dy = 0$ due to the periodicity of v and $\partial_{y_1} v$. Finally the variational formulation

$$\int_{Y_B} M^B \nabla_y \nabla_y^T v \; dy = -\int_{Y_B} F^B \nabla_y \nabla_y^T v \; dy$$

is fulfilled.

Problem $\mathcal{P}^M$: It is straightforward to verify that

$$\mathcal{L}^B_{\xi\zeta\gamma\delta} = -\frac{2\lambda}{4(\lambda+\mu)} \delta_{\xi 2}\delta_{\zeta 2}\delta_{\gamma 1}\delta_{\rho 1}$$

$$\widetilde{R}^M_{\alpha\beta\gamma\rho} = \frac{4\mu\ell_B a_B^3 \varepsilon^3}{3}\left(\frac{\lambda}{\lambda+2\mu}\delta_{\alpha\beta}\delta_{\gamma\rho} + \delta_{\alpha\gamma}\delta_{\beta\rho} - \frac{\lambda}{2(\lambda+\mu)}\left(\frac{\lambda}{\lambda+2\mu}\delta_{\alpha\beta}\delta_{\gamma 1}\delta_{1\rho} + \delta_{\alpha 2}\delta_{2\beta}\delta_{\gamma 1}\delta_{1\rho}\right)\right).$$

It then follows that

$$R^M = \begin{pmatrix} \widetilde{R}^M_{1111} & 0 \\ 0 & \dfrac{16\ell_B\mu}{3} \end{pmatrix} \text{ with } \widetilde{R}^M_{1111} = \frac{4\ell_B\mu a_B^3\varepsilon^3}{3(\lambda+2\mu)}(2\lambda+2\mu-\frac{\lambda^2}{2(\lambda+\mu)}).$$

The macroscopic forces are $f_1^M(x) = F(d(x))/\varepsilon^2$ and $f_2^M = 0$. Then multiplying the equation of u^M by ε and introducing $R^M_{11} = \varepsilon\widetilde{R}^M_{1111}$, one find that u^M is solution of the boundary value problem (48) and θ is solution of

$$\partial^2_{x_1x_1}\theta(x) = 0 \text{ for } x \in \omega,\ \theta(0,x_2) = \theta(1,x_2) = 0 \text{ for all } x_1 \in (0,1)$$

thus $\theta = 0$.

Problem $\mathcal{P}^C$: The calculations are exactly the same as those for the simple plate model in Section 6.1 excepted that x, L_E, u_3^P, ξ^P, Ξ_2^P, b^P, B_2^P, Ω_R, ω_R and H^P are replaced by y^C, L_F, u^C, ξ^C, Ξ_2^C, b^C, B_2^C, V_R, Y_R and H^C. Neglecting the variations of u^C with respect to y_1 it comes that u^C depends of x and y_2 only and is solution of the boundary value problem

$$\begin{aligned} \frac{\partial^4 u^C}{\partial y_2^4} &= 0 \text{ for } y_2^C \in (0,L_F),\ u^C = \frac{\partial u^C}{\partial y_2} = 0 \text{ for } y_2^C = 0 \\ -\ell_C R^P_{2222}\varepsilon^{-4}\frac{\partial^3 u^C}{\partial y_2^3} &= \xi^C \text{ and } \ell_C R^P_{2222}\varepsilon^{-4}(\frac{\partial^2 u^C}{\partial y_2^2} - \frac{\partial^3 u^C}{\partial y_2^3}y_2^C) = \Xi_2^C \text{ for } y_2^C = L_F \end{aligned} \tag{50}$$

and

$$\begin{aligned} \xi^C(x) &= F(d(x))/\varepsilon^2, \\ \Xi_2^C(x) &= |V_R|^{-1}\int_{Y^R}(a^C + h^0(y))y_2\ dy\ F(d(x))/\varepsilon^2 = \frac{|Y_R|H^C}{|V_R|}F(d(x))/\varepsilon^2. \end{aligned}$$

By introducing $m^C = \ell_C R^P_{2222}\varepsilon^{-3}$ The expression of u^C follows. Finally by using the relation $u^C(.,y_2) = d - u^M + \phi$ for $y_2^C = y_2^{Ctip}$ the equation (49) follows.

6.3 Numerical Simulation of the AFM Array

For numerical computation the algebraic equation (49) is replaced by

$$(d+\phi-u^M)(R+d-R\sin(\gamma))^2d^2 - (k^C)^{-1}G(d) = 0 \tag{51}$$

where $G(d) = \varepsilon^{-1}F(d)(R+d-R\sin(\gamma))^2d^2$. $F(d) = F^{vdW}(d) + F^{rep}(d)$ where the van der Waals F^{vdW} is defined in (42) from the potential (34) and the repulsive force F^{rep} is build from (43) on the same way. In order to avoid numerical errors due to the presence of large and small values in the system, we use the normalized functions and variables

$$\begin{gathered} x_1^* = x/L_1,\ x_2^* = x_2/L_2,\ u^{M*}(x^*) = u^M(x)/\phi_{scal},\ d^*(x^*) = d(x)/\phi_{scal}, \\ \phi^*(x^*) = \phi(x)/\phi_{scal},\ F^*(d^*) = L_1^4F(d^*\phi_{scal})/(R^M_{11}\phi_{scal}), \\ G^*(d^*) = G(d^*\phi_{scal})/\phi^3_{scal},\ R^* = R/\phi_{scal},\ k^* = k^C(y_2^{tip})\phi^2_{scal} \end{gathered}$$

so that (48) and (51) are replaced by

$$\begin{gathered} \partial^4_{x_1^*}u^{M*} = F^*(d^*) \text{ and } E(d^*,u^{M*}) = 0 \text{ in } (0,1)^2 \\ u^{M*}(x^*) = \partial_{x_1}u^{M*}(x^*) = 0 \text{ for all } x^* \in \{0,1\}\times(0,1) \end{gathered}$$

with $E(d^*, u^{M*}) = (d^* + \phi^* - u^{M*})(R^* + d^* - R^* \sin(\gamma))^2 (d^*)^2 - k^{*-1} G^*(d^*)$. The displacement u^{M*} is decomposed on the basis of eigenfunctions $\psi_m(x_1^*)$:

$$u^{M*}(x^*) = \sum_{n=1}^{N_u} U_n(x_2^*)\psi_n(x_1^*)$$

where

$$\partial^4_{x_1^*}\psi_n(x_1^*) = \lambda_n \psi_n(x_1^*) \text{ for all } x_1^* \in (0,1) \text{ and } \psi_n(x_1^*) = \partial_{x_1}\psi_n(x_1^*) = 0 \text{ for } x_1^* \in \{0,1\},$$

then

$$U_n(x_1^*) = \int_0^1 F^*(d^*(x^*))\psi_n(x_1^*)\ dx_1^*/\lambda_n. \tag{52}$$

The functions ϕ^* and d^* are decomposed on the normalized orthogonal Chebychev polynomials P_n on $(0,1)$:

$$\phi^*(x_1^*) = \sum_{n=1}^{N_\phi} \Phi_n(x_2^*)P_{n-1}(x_1^*) \text{ and } d^*(x_1^*) = \sum_{n=1}^{N_d} D_n(x_2^*)P_{n-1}(x_1^*).$$

Thus the second equation is replaced by

$$\mathcal{E}(D, \Phi, U) = 0$$

where

$$\mathcal{E}(D, \Phi, U) = E(\sum_{n=1}^{N_d} D_n(x_2^*)P_{n-1}(x_1^*), \sum_{n=1}^{N_\phi} \Phi_n(x_2^*)P_{n-1}(x_1^*), \sum_{n=1}^{N_u} U_n(x_2^*)\psi_n(x_1^*)).$$

The discretized system is solved by replacing U_n by its expression (52) and then by searching the minimum of $\int_0^1 \mathcal{E}^2(D, \Phi, U)\ dx_1^*$ with respect to D. The minimum search is conducted by combining a minimizing method relatively to D and a length line continuation with respect to the number of cells. The algorithm is initialized with a small number of cells where u^{M*} is close to zero. Then the number of cells is increased incrementally.

We have conducted computations with a square cell having a length of $\varepsilon = 50\mu m$. The other parameters are $L_C = 0.5$, $\ell_C^0 = 1/16$, $a_C = 1/40$, $y_2^{Ctip} = 7/16$, $L_F = 3/8$, $\ell_B = 1/4$, $a_B = 1/10$, $A = 1.25e-19J$, $\gamma = \pi/6$, $R = 10^{-7}m$, $\lambda = 6.1e11$, $\mu = 5.2e11$, $\phi_{scal} = 10^{-9}$ and finally the shape of the tip is chosen so that $(k^C(y_2^{tip}))^{-1} = 3e-8$. The number of cantilevers or equivalently the length of the array is a parameter chosen in each experiment. In the following we refer to three choices of ϕ^* corresponding to three values of N_ϕ :

$$\begin{aligned} N_\phi &= 1 : \phi^*(x_1^*) = \frac{\phi^{0*} + \phi^{1*}}{2}, \\ N_\phi &= 2 : \phi^*(x_1^*) = \phi^{0*} + (\phi^{1*} - \phi^{0*})x_1^*\ , \\ N_\phi &= 3 : \phi^*(x_1^*) = \phi^{0*} + 4\phi^{1*}x_1^*(1 - x_1^*) \end{aligned}$$

where $\phi^{0*} = -0.3$ and $\phi^{1*} = -0.4$.

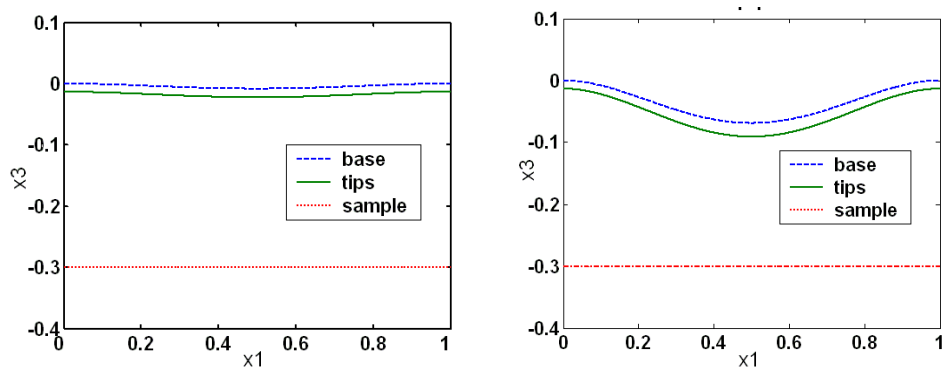

Figure 7: Distributions of u^{M*}, $u^{M*} + \overline{u}^{C*}$ and of ϕ^* as functions of x_1^* for 10, 16 cantilevers

Figure 7 represents the functions u^{M*}, $u^{M*} + \overline{u}^{C*}$ at the tip locations and of ϕ^* of $x_1^* \in (0, 1)$ in the case of a flat sample, $N_\phi = 1$, for two arrays having 10 and 16 cantilevers in the direction x_1. It is not surprising to observe that when the base length increases it deforms on a non negligible way in comparison with the total displacement of the tip.

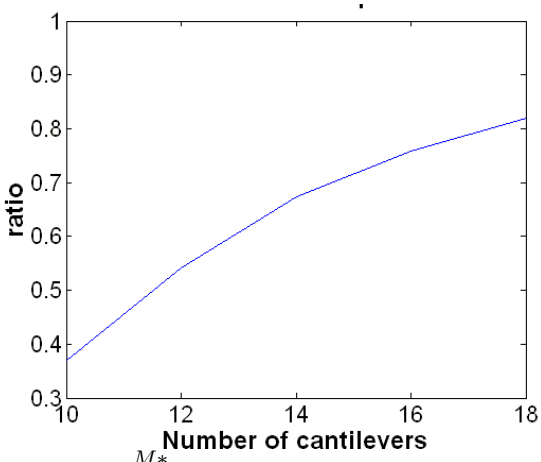

Figure 8: $\max_{x^*} \dfrac{u^{M*}}{u^{M*} + \overline{u}^{C*}}$ with respect to the number of cells

Figure 8 illsustrates how the maximum value over x_1^* of the ratio $\dfrac{u^{M*}}{u^{M*} + \overline{u}^{C*}}$ taken at the tips varies as a function of the number of cells for $N_\phi = 1$. Evidently this ratio tends to zero for a small number of cells but it also increases dramatically with the number of cells which means that in this case the tip displacement is more governed by the base displacement than by the the cantilever deflection.

$N_\phi \backslash N_d$	1	3	5	7	9
1	2.2	2.8	4.3	5.7	7.4
2	1.0	2.8	3.7	3.8	3.9
3	0.7	2.7	3.4	4.0	4.7

$N_\phi \backslash N_d$	1	3	5	7	9
1	1.5	2.1	3.6	4.9	5.8
2	1.0	2.1	3.6	4.6	4.7
3	0.6	2.5	3.4	4.0	4.1

Table 1: Err for 10 cells and 14 cells depending on N_ϕ and N_d

The quality of the approximation of d^* by using the Chebychev polynomials is also of interest. In table 1, we report the order of magnitude of the error on d^*

$$Err = -\log_{10} err \text{ where } err^2 = \frac{\int_0^1 (d^*_{N_d}(x_1^*) - d^*(x_1^*))^2 \, dx_1^*}{\int_0^1 (d^*(x_1^*))^2 \, dx_1^*}$$

as a function of the number N_d of polynomials used.

7 Appendix

In this appendix, we report some mathematical definitions and properties. The concept of weak and strong approximation are defined in Section 7.1. Then in Section 7.2 the two-scale transform of a function is defined and its elementary properties are stated. Weak approximations of first order and second order derivatives two-scale derivatives are derived in Section 7.3. In Section 7.4 we provide the expression of a volumic force which action is equivalent to a concentrated force when it is applied in the rigid part. This result is used in the examples of Sections 6.1 and 6.2. Finally a fundamental inequality used for the derivation of the two-scale model is stated and proved in Section 7.5.

7.1 Weak and strong Approximation

Consider an open set $A \in \mathbb{R}^n$, $w^\varepsilon \in L^2(A)$, a function depending on the parameter ε and a function $w^0 \in L^2(A)$ independent of ε. We say that $w^\varepsilon = w^0 + O(\varepsilon)$ weakly in $L^2(A)$ if $\int_A (w^\varepsilon - v^0)v \; dx = O(\varepsilon)$ for all $v \in L^2(A)$ and we say that the same equality holds strongly in $L^2(A)$ if $\int_A (w^\varepsilon - w^0)^2 \; dx = O(\varepsilon)$.

For example the oscillating function $\sin(\frac{x}{\varepsilon})$ can be approximated by zero in the weak sense but cannot be approximated by a function independent of ε in the strong sense.

7.2 Properties of the Two-Scale Transform

We state here some elementary properties of the two-scale transform. The proofs are elementary and are not detailed here. Some may be found in M. Lenczner and G. Senouci [11].

For $v, w \in L^1(\omega)$,

$$\widehat{v+w} = \widehat{v} + \widehat{w}, \; \widehat{vw} = \widehat{v}\widehat{w} \text{ and } \int_\omega v(x)dx = \int_{\omega \times Y} \widehat{v}(x,y)dydx$$

For $v \in L^2(\omega)$,

$$||v||_\omega = ||\widehat{v}||_{\omega \times Y}$$

and if $\nabla v \in L^2(\omega)$ then

$$\widehat{\nabla v} = \varepsilon^{-1} \nabla_y \widehat{v}.$$

For any $\varepsilon Y-$periodic part ω_x of ω (like ω_P) and Y_x its corresponding reference cell in Y, it follows that

$$\widehat{\chi_{\omega_x}} = \chi_{\omega \times Y_x}.$$

It is convenient to note that the two scale transform is a linear operator T defined from $L^2(\omega)$ to $L^2(\omega \times Y)$ by $Tu = \widehat{u}$. Its adjoint T^* is defined by

$$\int_\omega u(x)(T^*v)(x) \; dx = \int_{\omega \times Y} (Tu)(x,y)v(x,y) \; dxdy \tag{53}$$

for all $u \in L^2(\omega)$ and $v \in L^2(\omega \times Y)$. A direct computation shows that

$$T^*v(x) = \sum_i \varepsilon^{-d} \int_{Y_i^\varepsilon} v(z, \frac{x - x_i}{\varepsilon})dz \; \chi_{Y_i^\varepsilon}(x) = \sum_i \varepsilon^{-d} \int_{Y_i^\varepsilon} \overline{v}(z, \frac{x}{\varepsilon})dz \; \chi_{Y_i^\varepsilon}(x)$$

where the function $\overline{v}$ is defined on $\omega \times \frac{1}{\varepsilon}\omega$ by $\overline{v}(z,y) = \sum_i v(z, y - \frac{x_i}{\varepsilon})\chi_{Y_i^\varepsilon}(z)$. Apparently $\overline{v}$ is not continous on ω; however if v is extended as an $Y-$periodic function on $\mathbb{R}^d$ then $\overline{v}$ can be rewritten as

$$\overline{v}(z,y) = v(z, y - \frac{1}{2}) \text{ for } (z,y) \in \omega \times \frac{1}{\varepsilon}\omega \tag{54}$$

and has evidently the same periodicity with respect to its second variable and the same differentiability with respect to both variables as v. It is useful to make the remark that if v is $k+1$ times continuously differentiable with respect to its first variable then T^*v can be approximated up to the order k with an expansion in ε,

$$T^*v = \sum_{j=0}^{k} f_k \varepsilon^k + \varepsilon^k O(\varepsilon) \tag{55}$$

whose coefficients are some functions of $\overline{v}(x, \frac{x}{\varepsilon})$ and their derivatives. It turns out that the first coefficients are

$$\begin{aligned} f_1 &= \overline{v}(x, \frac{x}{\varepsilon}), \\ f_2 &= -X(x).\nabla_x \overline{v}(x, \frac{x}{\varepsilon}) \\ f_3 &= \frac{1}{2}X(x)\nabla_x \nabla_x^T \overline{v}(x, \frac{x}{\varepsilon})X(x) + \frac{1}{12}\Delta_x \overline{v}(x, \frac{x}{\varepsilon}) \end{aligned}$$

where $X = T^*(y)$. The calculation of these coefficients is straightforward. One starts by applying the Taylor formula to $\overline{v}$ at (x,y) with respect to its first variable: $\overline{v}(z,y) = \overline{v}(x,y) + \nabla_x \overline{v}(x,y)(z-x) + \frac{1}{2}(z-x)^T \nabla_x \nabla_x^T \overline{v}(x,y)(z-x) + \varepsilon^2 O(\varepsilon)$ for $x, z \in Y_i^\varepsilon$. Then one substitutes it in the expression of T^*v. The calculations of the integrals are carried out by using the decomposition $z - x = (z - x_i^\varepsilon) + (x_i^\varepsilon - x)$ and the identities $\int_{Y_i^\varepsilon} (z - x_i^\varepsilon)\, dz = 0$ and $\sum_i \chi_{Y_i^\varepsilon}(x) = 1$.

Conversely one deduces an approximation of $\overline{v}(x, \frac{x}{\varepsilon})$:

$$\overline{v}(x, \frac{x}{\varepsilon}) = T^*(v + \varepsilon(y.\nabla_x)v + \frac{\varepsilon^2}{2}(y.\nabla_x)^2 v - \frac{\varepsilon^2}{24}\Delta_x v)(x) + \varepsilon^2 O(\varepsilon), \tag{56}$$

which is derived by applying the second order approximation (55) and replacing $\nabla_x \nabla_x^T \overline{v}$, $\Delta_x \overline{v}$ with their zero order approximation and $\nabla_x \nabla_y^T \overline{v}$ with its first order approximation.

The two-scale transform is a linear operator that is well defined on functions. Its definition can also be extended to some generalized functions or distributions: v being such a generalized function Tv is defined formally by duality

$$\int_\omega \langle Tv, w \rangle_y \; dx = \langle v, T^*w \rangle_x$$

for all w belonging to a class of regular functions defined on $\omega \times Y$. From this definition the two-scale transform of

$$v(x) = g(x) \sum_i \delta_{x_i + \varepsilon y^0}(x)$$

Tv is found to be

$$Tv(x,y) = \varepsilon^{-d} Tg(x,y)\delta_{y^0}(y) \tag{57}$$

where $y^0 \in Y$, δ_ξ is the Dirac distribution in ξ and g is any regular function. Indeed,

$$\langle v, T^*w\rangle_x = \left\langle g(x)\sum_i \delta_{x_i+\varepsilon y^0}(x), \sum_j \varepsilon^{-d}\int_{Y_j^\varepsilon} \overline{w}(z,\frac{x}{\varepsilon})dz\ \chi_{Y_j^\varepsilon}(x)\right\rangle_x$$

$$= \sum_i g(x_i+\varepsilon y^0)\varepsilon^{-d}\int_{Y_i^\varepsilon} w(z,y^0)dz = \varepsilon^{-d}\sum_i\int_{Y_i^\varepsilon} Tg(z,y^0)w(z,y^0)dz$$
$$= \varepsilon^{-d}\int_\omega Tg(z,y^0)w(z,y^0)dz = \varepsilon^{-d}\int_\omega \left\langle Tg(z,y)\delta_{y^0}(y), w(z,y^0)\right\rangle_y\ dz.$$

This means that $Tv(z,y) = \varepsilon^{-d}Tg(z,y)\delta_{y^0}(y)$.

7.3 Approximations of the Two-Scale Transform of the Derivatives

The following results are stated in the general case where d is any positive integer, $\omega = \Pi_{i=1}^d(0,L_i)$ and $Y = (-\frac{1}{2},\frac{1}{2})^d$ with L_i some non negative numbers. The definitions of the cells Y_i^ε and of the two-scale transform (15) still hold.

Notation: Consider a $\varepsilon Y-$periodic set $\omega_1 \subset \omega$ with cells Y_{1i}^ε and the associated unit cell $Y_1 = \frac{1}{\varepsilon}(Y_i^\varepsilon - x_i^\varepsilon) \subset Y$. The intersection between the boundaries of Y_1 and of Y is denoted by γ_{per}, it corresponds to the location where the cells Y_{1i}^ε are connected. We take into account cases where the cells Y_{1i}^ε are connected to their neighbors in some directions but not in the others. Then the gradient splits in two parts $\nabla = \nabla^C + \nabla^{NC}$ where ∇^C and ∇^{NC} contain respectively the partial derivatives in the connectivity directions and in the directions without connectivity. In the same way, the components y and the unit outwards normal vectors n to a boundary ($\partial\omega$ or ∂Y_1) split as $y = y^C + y^{NC}$ and $n = n^C + n^{NC}$. The extremal cases where the cells Y_{1i}^ε are connected in all directions ($\nabla^C = \nabla$, $n^C = n$ and $y^C = y$) or in none of them ($\nabla^C = n^C = y^C = 0$) are encompassed by these notations. The part of the boundary $\partial\omega$ where the unit outward normal vector $n_x^C \neq 0$ is divided into γ_0^M where boundary conditions are applied and γ_1^M.

First order derivatives: Let u be a function defined on ω_1, depending on the parameter ε, vanishing on $\gamma_0^M \cap \partial\omega_1$ and such that its norms $||u||_{\omega_1}$ and $||\nabla u||_{\omega_1}$ are $O(1)$ with respect to ε. From the norm conservation through the two-scale transform, we already know that $||\widehat{u}||_{\omega\times Y_1}$ and $||\widehat{\nabla u}||_{\omega\times Y_1}$ are also $O(1)$. If, in any manner, it is known that $\widehat{u}$ admits an expansion with respect to ε on the form $\widehat{u} = u^0 + \varepsilon\widetilde{u}^1 + \varepsilon O(\varepsilon)$, at least in the weak sense, with u^0 and $\widetilde{u}^1$ independent of ε, then $u^0 = 0$ on γ_0, $\nabla_y u^0 = 0$ on $\omega\times Y_1$,

$$\widehat{\nabla u} = \nabla_x^C u^0 + \nabla_y u^1 + O(\varepsilon) \text{ on } \omega\times Y_1 \tag{58}$$

in the weak sense, $u^1 = \widetilde{u}^1 - y^C.\nabla_x^C u^0$, u^1 is $Y-$periodic on γ_{per}, $u^0 \in L^2(\omega)$, $\nabla_x^C u^0(x) \in L^2(\omega)^d$, $u^1 \in L^2(\omega\times Y_1)$ and $\nabla_y u^1 \in L^2(\omega\times Y_1)^d$.

Second order derivatives: In addition, we assume that $||\nabla\nabla^T u||_{\omega_1}$ is $O(1)$, that $\nabla u = 0$ on $\gamma_0^M \cap \partial\omega_1$ and that $\widehat{u} = u^0 + \varepsilon\widetilde{u}^1 + \varepsilon\widetilde{u}^2 + \varepsilon^2 O(\varepsilon)$, at least in the weak sense. It then follows that $||\widehat{\nabla\nabla^T u}||_{\omega\times Y_1}$ is $O(1)$, $\nabla_x u^0 = 0$ on γ_0, $\nabla_y\nabla_y^T u^1 = 0$, $\nabla_y^C u^1 = 0$,

$$\begin{aligned} \widehat{\nabla u} &= \nabla_x^C u^0 + \theta^{NC} + O(\varepsilon) \\ \text{and } \widehat{\nabla\nabla^T u} &= \nabla_x^C(\nabla_x^C)^T u^0 + \nabla_x^C(\theta^{NC})^T + (\nabla_x^C(\theta^{NC})^T)^T + \nabla\nabla^T u^2 + O(\varepsilon) \end{aligned} \tag{59}$$

on $\omega \times Y_1$ in the weak sense, $u^2 = \widetilde{u}^2 - y^C.\nabla_x^C \widetilde{u}^1 + (y^C.\nabla_x^C)^2 u^0$, u^2 and $\nabla_y u^2$ are $Y-$periodic on γ_{per}, $\theta^{NC} = \nabla_y^{NC} u^1$ which is independent of y, $\nabla_x^C (\nabla_x^C)^T u^0 \in L^2(\omega)^{d\times d}$ and $\nabla_x^C \nabla_y u^1$, $\nabla\nabla^T u^2 \in L^2(\omega \times Y_1)^{d\times d}$.

Strong variations, first order derivatives: In the case where the variations of u are sufficiently large that $||\nabla u||_{\omega_1}$ is not of order $O(1)$ but $||\varepsilon \nabla u||_{\omega_1}$ is $O(1)$ and $\widehat{u} = u^0 + O(\varepsilon)$, at least in the weak sense, then $\nabla_y u^0 \in L^2(\omega \times Y_1)$ and

$$\varepsilon \widehat{\nabla u}(x,y) = \nabla_y u^0 + O(\varepsilon) \tag{60}$$

in the weak sense.

Strong variations, second order derivatives: If in addition $||\varepsilon^2 \nabla\nabla^T u||_{\omega_1}$ is $O(1)$ then $\nabla_y \nabla_y^T u^0 \in L^2(\omega \times Y_1)$ and

$$\varepsilon^2 \widehat{\nabla\nabla^T u}(x,y) = \nabla\nabla^T u^0 + O(\varepsilon). \tag{61}$$

Here we sketch the proof of these approximations by indicating the calculation steps without going into precise mathematical justifications.

Proof for the first order derivative: The proof is decomposed into four steps.

(i) If $||\nabla u||_{\omega_1}$ is $O(1)$ then $\nabla_y u^0 = 0$. This comes from the properties of the two-scale transform recalled above: $\varepsilon ||\nabla u||_{\omega_1} = \varepsilon ||\widehat{\nabla u}||_{\omega\times Y_1} = ||\nabla_y \widehat{u}||_{\omega\times Y_1} = O(\varepsilon)$.

Next, we decompose $\widehat{\nabla u} = \widehat{\nabla^C u} + \widehat{\nabla^{NC} u}$ and compute each part separately.

(ii) The first term turns out to be approximated by

$$\widehat{\nabla^C u} = \nabla_x^C u^0 + \nabla_y^C u^1 + O(\varepsilon) \text{ on } \omega \times Y_1.$$

Consider a function $v(x,y)$ two times continuously differentiable with respect to x in $\omega \times Y_1$, vanishing for $y \in \partial Y_1 - \gamma_{per}$ and for $x \in \gamma_1^M$ and extended by zero for $y \in Y - Y_1$. We assume also that the function $\overline{v}$ defined from v by (54) is differentiable with respect to y. Then, E_{ω_1} denoting the operator of extension by zero from ω_1 to ω,

$$X = \int_{\omega\times Y} T E_{\omega_1} \nabla^C u.v \; dydx = \int_{\omega_1} \nabla^C u.T^* v \; dx = \int_{\omega_1} \nabla^C u(x).\overline{v}(x, \frac{x}{\varepsilon}) \; dx + O(\varepsilon)$$

due to the zero order approximation of $T^* v$ and the fact that $||\nabla u||_{\omega_1}$ is bounded. Applying the Green formula and taking into account that the product $u\; v$ vanishes on the boundary of ω it follows that

$$X = -\int_{\omega_1} u(x)(div_x^C \overline{v}(x, \frac{x}{\varepsilon}) + \varepsilon^{-1} div_y^C \overline{v}(x, \frac{x}{\varepsilon})) \; dx + O(\varepsilon).$$

Applying the approximation (55) at the zero order to $div_x^C \overline{v}(x, \frac{x}{\varepsilon})$ and at the first order to $div_y^C \overline{v}(x, \frac{x}{\varepsilon})$ yields

$$X = -\int_{\omega_1} u \; T^*(div_x^C v + \varepsilon^{-1} div_y^C v + y.\nabla_x div_y^C v) \; dx + O(\varepsilon)$$

or equivalently

$$X = -\int_{\omega\times Y_1} \widehat{u} \; (div_x^C v + \varepsilon^{-1} div_y^C v + y.\nabla_x div_y^C v) \; dxdy + O(\varepsilon)$$

Since $\widehat{u} = u^0 + \varepsilon\widetilde{u}^1 + \varepsilon O(\varepsilon)$ and $\nabla_y^C u^0 = 0$, applying the Green formula in the reverse sense yields

$$\begin{aligned}\int_{\omega\times Y} \widehat{\nabla^C u}.v\ dydx &= \int_{\omega\times Y_1} (\nabla_x^C u^0 + \nabla_y^C u^1).v\ dydx \\ &\quad - \int_{\omega\times\gamma_{per}} u^1 v.n_y^C\ ds(y)dx - \int_{\gamma_0^M\times Y_1} u^0 v.n_x^C\ ds(y)dx + O(\varepsilon)\end{aligned} \tag{62}$$

with $u^1 = \widetilde{u}^1 - y^C.\nabla_x^C u^0$. From the conditions imposed on v, it follows that all the boundary terms except those on $\omega\times\gamma_{per}$ vanish. Here we have used the fact that $\int_{Y_1} u^0\ y^{NC}.\nabla_x div_y^C v\ dy = 0$. Reducing the choice of functions to those satisfying $v = 0$ on $\omega\times\gamma_{per}$ and on $\gamma_0^M\times Y_1$ gives

$$\int_{\omega\times Y} \widehat{\nabla^C u}.v\ dydx = \int_{\omega\times Y_1} (\nabla_x^C u^0 + \nabla_y^C u^1).v\ dydx + O(\varepsilon)$$

which holds only for the above mentioned v. However, from a density argument this is valid also for all $v\in L^2(\omega\times Y_1)$. So we conclude that the equality $\widehat{\nabla^C u} = \nabla_x^C u^0 + \nabla_y^C u^1 + O(\varepsilon)$ holds in the weak sense.

(iii) As a by-product of (62) it follows that u^1 is $Y-$periodic on γ_{per} and $u^0 = 0$ on γ_0^M. Restarting from (62) with $v = 0$ on $\gamma_0^M\times Y_1$ it follows that

$$\int_{\omega\times\gamma_{per}} u^1 v.n_y^C\ ds(y)dx = O(\varepsilon)$$

which says that u^1 is $Y-$periodic on γ_{per}. Finally for an v it remains

$$\int_{\gamma_0^M\times Y_1} u^0 v.n_x^C\ ds(y)dx = O(\varepsilon)$$

that says that $u^0 = 0$ on γ_0^M.

(iv) The expression of the complementary $\widehat{\nabla^{NC} u}$ is

$$\widehat{\nabla^{NC} u} = \nabla_y^{NC} u^1 + O(\varepsilon).$$

Indeed $\widehat{\nabla^{NC} u} = \varepsilon^{-1}\nabla_y^{NC}\widehat{u} = \varepsilon^{-1}\nabla_y^{NC}(u^0 + \varepsilon\widetilde{u}^1) + O(\varepsilon) = \nabla_y^{NC} u^1 + O(\varepsilon)$.

This completes the derivation of (58).

Sketch of the proof for the second order derivative: From $||\nabla\nabla^T u||_{\omega_1} = O(1)$ it follows that $\nabla_y\nabla_y^T u^1$ vanishes, then u^1 is affine with respect to y and $\theta^{NC} = \nabla_y^{NC} u^1$ is independent of y. Furthermore, u^1 being periodic on γ_{per} implies that it is independent of y^C or in other words that $\nabla_y^C u^1 = 0$. The proof of (59) follows the same arguments (58) except that v is a symmetric $d\times d$ matrix. The matrix of second order derivative splits in three parts $\nabla\nabla^T u = (\nabla^C)^2 u + \nabla^C(\nabla^{NC})^T u + \nabla^{NC}(\nabla^C)^T u + (\nabla^{NC})^2 u$.

(i) The approximation of the first term

$$\widehat{\nabla^C(\nabla^C)^T u} = \nabla_x^C(\nabla_x^C)^T u^0 + \nabla_y^C(\nabla_y^C)^T u^2 + O(\varepsilon) \text{ on } \omega\times Y_1 \tag{63}$$

and of the boundary conditions on γ_0^M and on γ_{per} are derived through the same calculation. The second order approximation (55) of T^*v leads, after few lines of simple calculation, to

$$\int_{\omega\times Y} \widehat{\nabla^C(\nabla^C)^T}u \ : \ : v\ dydx = \int_{\omega\times Y_1} (\nabla_x^C(\nabla_x^C)^T u^0 + \nabla_y^C(\nabla_y^C)^T u^2) :: v\ dydx$$
$$+ \int_{\omega\times\gamma_{per}} [u^1(div_x^C v) + u^2(div_y^C v) - (\nabla_y^C u^2)^T v].n_y^C\ ds(y)dx + O(\varepsilon).$$

The formula (63) as well as the boundary conditions follow.

(ii) The second term $\widehat{\nabla^C\nabla^{NC}}u$ is approximated by

$$\widehat{\nabla^C(\nabla^{NC})^T}u = \nabla_x^C(\theta^{NC})^T + \nabla_y^{NC}(\nabla_y^C)^T u^2 + O(\varepsilon). \tag{64}$$

Here ∇^{NC} is applied to u and ∇^C is transposed on the test function. Following the calculation and using the fact that $\nabla_y^{NC}(y^C.\nabla_x^C u^0) = 0$ the formula

$$\int_{\omega\times Y} \widehat{\nabla^C(\nabla^{NC})^T}u :: vdydx = \int_{\omega\times Y_1} (\nabla_x^C(\theta^{NC})^T + \nabla_y^{NC}(\nabla_y^C)^T u^2) :: v\ dydx + O(\varepsilon)$$

arises when $v = 0$ on $\omega\times\gamma_{per}$ and on $\partial\omega\times Y_1$. This provides immediately (64).

(iii) The third term $\widehat{\nabla^{NC}(\nabla^C)^T}u$ is equal to the second term transposed so its approximation is equal to the transposed approximation of the second term.

(iv) The derivation of the formula for the fourth term

$$\widehat{(\nabla^{NC})^2}u = \nabla_y^{NC}(\nabla_y^{NC})^T u^2 + O(\varepsilon) \text{ on } \omega\times Y_1 \tag{65}$$

is straightforward.

Proof for the strong variations case: For proving (60) and (61), let us recall that $\varepsilon\widehat{\nabla u} = \nabla_y\widehat{u}$ and $\varepsilon^2\widehat{\nabla\nabla^T u} = \nabla_y\nabla_y^T\widehat{u}$, so using the expansion of $\widehat{u}$ leads directly to the results.

7.4 The volumic force associated to a concentrated force in the rigid part

Consider a concentrated force $F\delta_{x^{tip}}(x)$ applied to the extremity of the rigid part Ω_R in the example 6.1 where F is any vector of $\mathbb{R}^3$. We may prove that the force

$$f(x) = \frac{F}{|\Omega_R|} + \mathcal{F}\times(x - x^G)$$

produces the same effect on the rigid part as the concentrated force where x^G is the gravity center of Ω^R and $\mathcal{F} = A^{-1}((x^{tip} - x^G)\times F)$. The associated forces in the plate model are

$$\begin{aligned}
f^P(x) &= \frac{a+h(x)}{|\Omega_R|}[F_3 + \mathcal{F}.(x_2, -x_1, 0)^T] \\
g_1^P(x) &= \frac{a^2 - h^2(x)}{2|\Omega_R|}F_2 + \mathcal{F}.(0, \frac{a-h(x)}{2}, -x_2)^T \\
g_2^P(x) &= \frac{a^2 - h^2(x)}{2|\Omega_R|}F_2 + \mathcal{F}.(-\frac{a-h(x)}{2}, 0, -x_1)^T.
\end{aligned}$$

We remark that, if F is colinear to $x^{tip} - x^G$ then $\mathcal{F} = 0$. Furthermore if $F = (0, 0, F_3)^T$ the forces in the thin plates are

$$f^P(x) = \frac{a + h(x)}{|\Omega_R|} F_3 \text{ and } g^P_\alpha = 0.$$

Here A is the 3×3 matrice with coefficients

$$A_{ii} = \sum_{j \neq i} \int_{\Omega_R} (x_j - x^G_j)^2 \, dx \text{ and } A_{ij} = -\int_{\Omega} (x_i - x^G_i)(x_j - x^G_j) \, dx \text{ for } i \neq j.$$

To prove this, one search the function f under the form $f(x) = d + D \times (x - x^G)$ with d and D in $\mathbb{R}^3$ which satisfies

$$\int_{\Omega_R} f(x) v(x) \, dx = F.v(x^0)$$

for $v(x) = c + C \times (x - x^G)$ and all c and C in $\mathbb{R}^3$. By posing $C = 0$ it follows that $d = F/|\Omega_R|$ and then by posing $c = 0$:

$$\int_{\Omega_R} (C \times (x - x^G)).(D \times (x - x^G)) \, dx = (C \times (x^0 - x^G)).F$$

or equivalently

$$C. \int_{\Omega_R} (x - x^G) \times (D \times (x - x^G)) \, dx = C.((x^0 - x^G) \times F)$$

then

$$\int_{\Omega_R} (x - x^G) \times (D \times (x - x^G)) \, dx = (x^0 - x^G) \times F$$

from which the expression $D = A^{-1}((x^0 - x^G) \times F)$ follows. The expressions of f^P and g^P are derived straightfowardly.

7.5 An Inequality

Lemma 2 *For all $v \in H^1(\omega_P)$ such that $v = 0$ on γ_0^ε it follows that*

$$||v||_{\omega_P} \leq C ||\chi_{\omega_B} \nabla v + \chi_{\omega_F} \varepsilon \nabla v||_{\omega_P}. \tag{66}$$

Proof. (i) First we establish that there exists a constant $C_1 > 0$ such that for all $v \in H^1(Y)$ $||v||^2_{Y_C} \leq C_1(||v||^2_{Y_B} + ||\nabla v||^2_Y)$. This is proven similarly to the classical Poincaré inequalities.

(ii) Then we establish that there exists a constant $C_2 > 0$ such that for all $v \in H^1_{\gamma_0^\varepsilon}(\omega_P)$ and all $\varepsilon > 0$, $||v||^2_{\omega_P} \leq C_3 ||\chi_{\omega_B}(\partial_{x_1} v, \varepsilon \partial_{x_2} v) + \varepsilon \nabla v||^2_{\omega_P}$. Let us start from the previous inequality and for each i let us apply the change of variable that maps Y towards Y_i^ε for each. This leads to a family of inequality that we sum over i. It follows that for all $v \in H^1(\omega_P)$:

$$||v||^2_{\omega_C} \leq C_1(||v||^2_{\omega_C} + ||\varepsilon \nabla v||^2_{\omega_P}). \tag{67}$$

By another way, let us introduce a scaling of ω_B by a factor of $n = 1/\varepsilon$ in the direction x_2 only. This leads to a family $\widehat{\omega}$ of n strips with length equal to 1 in the x_1 direction and of the

order of one in the second direction. The classical Poincaré inequality may be applied to each of them which in turn by summation over the n strips yields $||v||^2_{\widehat{\omega}} \leq C_2||\nabla v||^2_{\widehat{\omega}}$ provided that $v \in H^1_{\widehat{\gamma}_0^\varepsilon}(\widehat{\omega}^\varepsilon)$. Here $\widehat{\gamma}_0^\varepsilon$ is obtained through the dilatation of γ_0^ε by a factor $1/\varepsilon$. By reversing the scaling, it follows that for all $v \in H^1_{\gamma_0^\varepsilon}(\omega)$,

$$||v||^2_{\omega_C} \leq C_2||(\partial_{x_1} v, \varepsilon\partial_{x_2} v)||^2_{\omega_C}. \tag{68}$$

Combining (67-68) yields (ii)

(iii) The desired result is a direct consequence of (ii). ■

Conclusion: We have derived two-scale models of AFM Arrays which take into account the deformations of the base coupled with those of the cantilevers. The first model is a general one and can be discretized with a Finite Element Method for both the macroscopic domain and the reference cell. The second model is a particular case where hand calculations have been pushed at their limit, so it has the form of a Euler Bernoulli beam equation, associated to the base, coupled with a nonlinear algebraic equation for the cantilevers. They do not require an heavy Finite Elements implementation and may provide an efficient model for a designer. The derivation of the general model is based on asymptotic approach which guaranties a good confidence in its results. Let us review the features of the general model. The cantilevers are modeled with a Love-Kirchhoff thin plate model which allows to describe general plate flexions encountered for example in nanomanipulation, their tip is rigid, the atomic forces are really applied to the extremity of the tip and the base is assumed to be much stiffer than the cantilevers which simplifies significantly the model. The results show that even for a small number of cantilevers, the mechanical displacement of the base cannot be neglected in a design process. Our perspectives consist in completing this work by several aspects including the dynamics, realistic shapes of the sample and control of the whole system.

References

[1] Destuynder, P.; Salaun, M.. Mathematical analysis of thin plate models, Springer, Berlin, 1996.

[2] Ciarlet, P.G.. Mathematical elasticity. Vol. II, North-Holland, Amsterdam, 1997.

[3] Sanchez-Palencia, E.. Nonhomogeneous media; vibration theory, Lecture Notes in Phys., 127, Springer, Berlin, 1980.

[4] Bensoussan, A; Lions, J-L; Papanicolaou, G.. Asymptotic analysis for periodic structures, North-Holland, Amsterdam, 1978.

[5] Allaire, G.. SIAM J. Math. Anal., v 23 (1992), n 6, 1482-1518.

[6] Canon, E.; Lenczner, M.. Math. Comput. Modelling, v 26 (1997), n 5, 79-106.

[7] Nguetseng, G.. SIAM J. Math. Anal., v 20 (1989), n 3, 608-623.

[8] Cioranescu, D.; Damlamian, A.; Griso, G.. C. R. Math. Acad. Sci. Paris, v 335 (2002), n 1, 99-104.

[9] Casado-Diaz, J.. Two-scale convergence for nonlinear Dirichlet problems in perforated domains. Proc. Roy. Soc. Edinburgh Sect. A, v 130, (2000), n 2, 249□276.

[10] Lenczner, M.; Mercier, D.. Multiscale Model. Simul. v 2 (2004), n 3, 359-397.

[11] Lenczner, M.; Senouci-Bereksi, G.. Math. Models Methods Appl. Sci., v 9 (1999), n 6, 899-932.

[12] Fung R.F.; Huang S.. Dynamic modeling; vibration analysis of the atomic force microscope. Transactions of the ASME. Journal of Vibration; Acoustics, v 123, n 4, (2001), p 502-9.

[13] Drakova, D.. Theoretical modelling of scanning tunnelling microscopy, scanning tunnelling spectroscopy; atomic force microscopy. Reports on Progress in Physics, v 64, n 2, (2001), p 205-90.

[14] Giessibl, F.J.. Advances in atomic force microscopy. Reviews of Modern Physics, v 75, n 3, (2003), p 949-83.

[15] Lenczner, M.. Homogenization of an electric circuit. Comptes Rendus de l'Academie des Sciences, Serie II, v 324, n 9, (1997), p 537-42.

[16] Stark, R.W.; Schitter, G.; Stark, M.; Guckenberger, R.; Stemmer, A. State-space model of freely vibrating and surface-coupled cantilever dynamics in atomic force microscopy. Physical Review B (Condensed Matter and Materials Physics), v 69, n 8, (2004), p 85412-1-9.

[17] Gotsmann, B., Seidel, C.; Anczykowski, B.; Fuchs, H. Conservative and dissipative tip-sample interaction forces probed with dynamic AFM. Physical Review B (Condensed Matter), v 60, n 15, (1999), p 11051-61.

[18] Vinogradova, O.I., Butt, H.-J.; Yakubov, G.E.; Feuillebois, F. Dynamic effects on force measurements. I. Viscous drag on the atomic force microscope cantilever. Review of Scientific Instruments, v 72, n 5, (2001), p 2330-9.

[19] Lobontiu, N.; Garcia, E. Two microcantilever designs: lumped-parameter model for static and modal analysis. Journal of Microelectromechanical Systems, v 13, n 1, (2004), p 41-50.

[20] Jalili, N.; Dadfarnia, M.; Dawson, D.M. A fresh insight into the microcantilever-sample interaction problem in non-contact atomic force microscopy. Transactions of the ASME. Journal of Dynamic Systems, Measurement and Control, v 126, n 2, (2004), p 327-35.

[21] Garcia, R.; Perez, R. Dynamic atomic force microscopy methods. Surface Science Reports, v 47, n 6-8, (2002), p 197-301.

[22] Elmer, F.-J.; Dreier, M. Eigenfrequencies of a rectangular atomic force microscope cantilever in a medium. Journal of Applied Physics, v 81, n 12, 15 June (1997), p 7709-14.

[23] Sader, J.E. Frequency response of cantilever beams immersed in viscous fluids with applications to the atomic force microscope. Journal of Applied Physics, v 84, n 1, 1 (1998), p 64-76.

[24] Napoli, M.; Wenhua Zhang; Turner, K.; Bamieh, B. Characterization of electrostatically coupled microcantilevers. Journal of Microelectromechanical Systems, v 14, n 2, (2005), p 295-304. A capacitive microcantilever: modelling, validation, and estimation using current measurements.

[25] Napoli, M.; Bamieh, B.; Dahleh, M. Optimal control of arrays of microcantilevers. Transactions of the ASME. Journal of Dynamic Systems, Measurement and Control, v 121, n 4, (1999), p 686-90.

[26] Argento, C. and French, R.H. Parametric tip model and force□distance relation for Hamaker constant determination from atomic force microscopy, *Journal of Applied Physics*, v 11, n 1, (1996), p 6081-6090.

[27] Argento, C., Jagota, A., and Carter, W.C., Surface formulation for molecular interactions of macroscopic bodies, *Journal of the Mechanics and Physics of Solids,* v 45, n 7, (1997), p 1161-1183.

[28] J. Israelachvili, *Intermolecular and Surface Forces: Second Edition,* Academic Press, London, 1992.

[29] Lang, H. P.; Hegner, M.; Gerber, C. Cantilever array sensors. Materials Today, v 8, n 4, (2005), p 30-36.

[30] Fasching, R. J.; Tao, Y.; Prinz, F. B.. Cantilever tip probe arrays for simultaneous SECM and AFM analysis. Sensors and Actuators, B: Chemical, v 108, n 1-2, (2005), p 964-972.

[31] Nugaeva, N.; Gfeller, K. Y.; Backmann, N.; Lang, H. P.; Duggelin, M.; Hegner, M. Micromechanical cantilever array sensors for selective fungal immobilization and fast growth detection. Biosensors and Bioelectronics, v 21, n 6, Dec 15, 2005, p 849-856.

[32] Volden, T.; Zimmermann, M.; Lange, D.; Brand, O.; Baltes, H.. Dynamics of CMOS-based thermally actuated cantilever arrays for force microscopy. Sensors and Actuators, A: Physical, v 115, n 22, (2004), p 516-52.

[33] Xu, T.; Bachman, M.; Zeng, F.; Li, G.. Polymeric micro-cantilever array for auditory front-end processing. Sensors and Actuators, A: Physical, v 114, n 2-3,(2004), p 176-182.

[34] Yang, Z.; Li, X.; Wang, Y.; Bao, H.; Liu, M.. Micro cantilever probe array integrated with Piezoresistive sensor. Microelectronics Journal, v 35, n 5, (2004), p 479-483.

[35] Kim, Y.; Nam, H.; Cho, S.; Hong, J.; Kim, D.; Bu, J. U.. PZT cantilever array integrated with piezoresistor sensor for high speed parallel operation of AFM. Sensors and Actuators, A: Physical, v 103, n 1-2, (2003), p 122-129.

[36] Saya, D.; Fukushima, K.; Toshiyoshi, H.; H., G.; Fujita, H.; Kawakatsu, H.. Fabrication of single-crystal Si cantilever array. Sensors and Actuators, A: Physical, v 95, n 2-3, (2002), p 281-287.

[37] Kim, B.H.; Prins, F.E.; Kern, D.P.; Raible, S.; Weimar, U.. Multicomponent analysis and prediction with a cantilever array based gas sensor. Sensors and Actuators, B: Chemical, v 78, n 1-3, (2001), p 12-18.

[38] Battiston, F.M.; Ramseyer, J.-P.; Lang, H.P.; Baller, M.K.; Gerber, C.; Gimzewski, J.K.; Meyer, E.; Guntherodt, H.-J.. A chemical sensor based on a microfabricated cantilever array with simultaneous resonance-frequency and bending readout. Sensors and Actuators, B: Chemical, v 77, n 1-2, (2001), p 122-131.

[39] Chow, E.M.; Soh, H.T.; Lee, H.C.; Adams, J.D.; Minne, S.C.; Yaralioglu, G.; Atalar, A.; Quate, C.F.; Kenny, T.W.. Integration of through-wafer interconnects with a two-dimensional cantilever array. Sensors and Actuators A (Physical), v A83, n 1-3, (2000), p 118-23.

[40] Rudnitsky, R.G.; Chow, E.m.; Kenny, T.W.. Rapid biochemical detection and differentiation with magnetic force microscope cantilever arraysSensors and Actuators A (Physical), v A83, n 1-3, (2000), p 256-62.

[41] Baller, M.K.; Lang, H.P.; Fritz, J.; Gerber, Ch.; Gimzewski, J.K.; Drechsler, U.; Rothuizen, H.; Despont, M.; Vettiger, P.; Battiston, F.M.; Ramseyer, J.P.; Fornaro, P.; Meyer, E.; Guntherodt, H.-J.. Cantilever array-based artificial nose. Ultramicroscopy, v 82, n 1, (2000), p 1-9.

[42] Lutwyche, M.; Andreoli, C.; Binnig, G.; Brugger, J.; Drechsler, U.; Haberle, W.; Rohrer, H.; Rothuizen, H.; Vettiger, P.; Yaralioglu, G.; Quate, C.. 5×5 2D AFM cantilever arrays a first step towards a Terabit storage device. Sensors and Actuators A (Physical), v A73, n 1-2, (1999), p 89-94;

[43] Young-Sik Kim; Sunyong Lee, C.; Won-Hyeog Jin; SeongSoo Jang; Hyo-Jin Nam; Jong-Uk Bu. 100×100 thermo-piezoelectric cantilever array for SPM nano-data-storage application. Sensors and Materials, v 17, n 2, (2005), p 57-63.

[44] Kakushima, K.; Watanabe, T.; Shimamoto, K.; Gouda, T.; Ataka, M.; Mimura, H.; Isono, Y.; Hashiguchi, G.; Mihara, Y.; Fujita, H.. Japanese Journal of Applied Physics, v 43, n 6B, (2004), p 4041-4.

[45] Graf, M.J.; Opeil, C.P.; Huber, T.E.. Magnetic anisotropy and de Haas-van Alphen oscillations in a Bi microwire array studied via cantilever magnetometry at low temperatures. Journal of Low Temperature Physics, v 134, n 5-6, (2004), p 1055-68.

[46] Yu Xiaomei; Zhang Dacheng; Li Ting; Wang Xiaobao; Ruan Yong; Du Xianfeng. Fabrication and analysis of micromachined cantilever array. Chinese Journal of Semiconductors, v 24, n 8, (2003), p 861-5.

[47] Srinivasan, P.; Beyette, F.R., Jr.; Papautsky, I.. Micromachined arrays of cantilevered glass probesd. Applied Optics, v 43, n 4, (2004), p 776-82.

[48] Bullen, D.; Sung-Wook Chung; Xuefeng Wang; Jun Zou; Mirkin, C.A.; Chang Liu. Parallel dip-pen nanolithography with arrays of individually addressable cantilevers. Applied Physics Letters, v 84, n 5, (2004), p 789-91.

[49] Calleja, M.; Tamayo, J.; Johansson, A.; Rasmussen, P.; Lechuga, L.M.; Boisen, A.. Polymeric cantilever arrays for biosensing applications. Sensor Letters, v 1, n 1, (2003), p 20-4.

[50] Abedinov, N.; Popov, C.; Yordanov, Z.; Ivanov, T.; Gotszalk, T.; Grabiec, P.; Kulisch, W.; Rangelow, I.W.; Filenko, D.; Shirshov, Yu.. Chemical recognition based on micromachined silicon cantilever array. Journal of Vacuum Science; Technology B, v 21, n 6, (2003), p 2931-6.

[51] Dragoman, D.; Dragoman, M.. Biased micromechanical cantilever arrays as optical image memory. Applied Optics, v 42, n 8, (2003), p 1515-19.

[52] Arntz, Y.; Seelig, J.D.; Lang, H.P.; Zhang, J.; Hunziker, P.; Ramseyer, J.P.; Meyer, E.; Hegner, M.; Gerber, C.. Label-free protein assay based on a nanomechanical cantilever array. Nanotechnology, v 14, n 1, (2003), p 86-90.

[53] Schaffer, T. E.. Force spectroscopy with a large dynamic range using small cantilevers and an array detector. Journal of Applied Physics, v 91, n 7, (2002), p 4739.

[54] Abedinov, N.; Grabiec, P.; Gotszalk, T.; Ivanov, Tz.; Voigt, J.; Rangelow, I.W.. Micromachined piezoresistive cantilever array with integrated resistive microheater for calorimetry and mass detection. Journal of Vacuum Science and Technology, Part A: Vacuum, Surfaces and Films, v 19, n 6, (2001), p 2884-2888.

[55] Cheng, H.-M.; Ewe, M.T.S.; Chiu, G.T.-C.; Bashir, R.. Modeling and control of piezoelectric cantilever beam micro-mirror and micro-laser arrays to reduce image banding in electrophotographic processes. Journal of Micromechanics and Microengineering, v 11, n 5, (2001), p 487-98.

[56] Green, J. D.; Lee, G. U.. Atomic force microscopy with patterned cantilevers and tip arrays: Force measurements with chemical arrays. Langmuir, v 16, n 8, (2000), p 4009-4015.

[57] Min Y. ; Lin, H.; Dedrick, D.E.; Satyanarayana, S.; Majumdar, A.; Bedekar, A.S.; Jenkins, J.W.; Sundaram, S.. A 2-D microcantilever array for multiplexed biomolecular analysis. Journal of Microelectromechanical Systems, v 13, n 2, (2004), p 290-9.

[58] Drechsler, U.; Burer, N.; Despont, M.; Durig, U.; Gotsmann, B.; Robin, F.; Vettiger, P.. Cantilevers with nano-heaters for thermomechanical storage application. Microelectronic Engineering, v 67-68, (2003), p 397-404.

[59] Tian, F.; Hansen, K. M.; Ferrell, T. L.; Thundat, T.; Hansen, D. C.. Dynamic microcantilever sensor for discerning biomolecular interactions. Analytical Chemistry, v 77, n 6, (2005), p 1601-1606.

[60] Hansen, K.M.; Ji, H.-F.; Wu, G.; Datar, R.; Cote, R.; Majumdar, A.; Thundat, T.. Cantilever-based optical deflection assay for discrimination of DNA single-nucleotide mismatches. Analytical Chemistry, v 73, n 7, (2001), p 1567-1571.

[61] Pepper, J.; Noring, R.; Klempner, M.; Cunningham, B.; Petrovich, A.; Bousquet, R.; Clapp, C.; Brady, J.; Hugh, B.. Detection of proteins and intact microorganisms using microfabricated flexural plate silicon resonator arrays. Sensors and Actuators, B: Chemical, v 96, n 3, (2003), p 565-575.

[62] King, W. P.; Kenny, T. W.; Goodson, K. E.; Cross, G. L.W.; Despont, M.; Durig, U. T.; Rothuizen, H.; Binnig, G.; Vettiger, P.. Design of atomic force microscope cantilevers for combined thermomechanical writing and thermal reading in array operation. Journal of Microelectromechanical Systems, v 11, n 6, (2002), p 765-774.